Synthesis and Characterization of Multifunctional Polymer-Derived SiOCN

Van Lam Nguyen

Advisor: Prof. Gian Domenico Sorarù

April 2015

Synthesis and Characterization of Multifunctional Polymer-Derived SiOCN

Van Lam Nguyen

E-mail: vanlam.nguyen@unitn.it

Approved by:

Ph.D. Commission:

Prof. Gian Domenico Sorarù,
Advisor
Department of Industrial
Engineering
University of Trento, Italy.

Prof. Gian Domenico Sorarù,
Department of Industrial
Engineering
University of Trento, Italy.

Prof. Ralf Riedel,
Department of Materials Science
Technical University of Darmstadt,
Germany.

Prof. Sabine Fuchs,
Department of Traumatology
University Hospital Schleswig-
Holstein, Campus Kiel, Germany.

To my family

Table of Contents

Abstract

This PhD thesis focuses on the synthesis and characterization of multifunctional polymer-derived SiOCN ceramics. The main objective is to synthesize N-doped silicon oxycarbides (SiOCs), to characterize their structure and their properties (mainly electrical conductivity) and correlate them with the presence of N in the structure. We also aim to understand how the architecture of the starting polymer can influence the retention of N into the SiOC structure.

First, N-doped SiOC polymer precursors were synthesized via hydrosilylation reaction between Si-H groups present in a commercial polysiloxane (PHMS) and –CH=CH$_2$ groups of three different commercial N-containing compounds. The structural characterization of as-synthesized preceramic polymer precursor was investigated by FT-IR and NMR. Thermal degradation was studied by TGA. The results show that the architecture of the polymer precursors plays an important role on the pyrolythic transformation.

Then, SiOCN ceramics were obtained by pyrolysis of the as-synthesized polymer precursors in nitrogen atmosphere at various temperatures for 1h using a tubular furnace. Subsequently, high temperature structural evolution was studied using combined techniques such as XRD, FT-IR, NMR, Elemental analysis, and XPS. The obtained results show that the type of N-containing compounds impacts on the crystallization behavior of the final ceramics. Elemental analysis clearly indicates that N is present in the SiOC matrix and the degree of N retention after pyrolysis is related to the type of N-containing starting compounds.

XPS data indicate that N-C bonds are present in the SiOC ceramic samples even if only N-Si bonds exist in the starting N-containing precursor. However, a larger fraction of N-C bonds is present in the final SiOCN ceramic when N atoms form bonds with sp^2 carbon atoms in the pre-ceramic polymer.

We have also studied electrical and optical properties of the SiOCNs. Electrical conductivity of the powdered ceramic samples was determined using powder-solution-composite technique. The results show an increase in room temperature AC conductivity of three orders of magnitude, from $\approx 10^{-5}$ (S/cm) to $\approx 10^{-2}$ (S/cm), with increasing pyrolysis temperature from 1000 to 1400 °C. Furthermore, the electrical conductivity of the SiOCN ceramic derived from N-C bond bearing precursor is three to five times higher than that of the sample derived from N-Si containing precursor at each pyrolysis temperature. The combined structural study by Raman spectroscopy and chemical analysis suggests that the increase of electrical conductivity with the pyrolysis temperature is due to the sp^3-to-sp^2 transition of the amorphous carbon phase. The higher conductivity of the amine-derived SiOCN is also discussed considering features like the volume % of the free-carbon phase and its possible N-doping. Fluorescence of the SiOCN samples treated at low temperatures, 400 and 600 °C, has been studied. The spectra show that the heated precursors fluoresce in the visible range with a dominant blue emission. Since the non-heated polymer precursors do not fluoresce, emitting centers must be formed during the polymer-to-ceramic transformation and associated with the structural changes. The origin of the luminescence could be originated from defects related to C, O and/or Si.

Finally, we investigated the gas sensing behavior of the SiOCNs pyrolyzed at low and high temperatures. Regarding the electrical gas sensing of the SiOCN ceramics pyrolyzed at 1400 °C, the response to two target gases NO_2 and H_2 was tested by *in situ* DC conductance measurements at operating temperatures from 200 to 550 °C. The SiOCN ceramics are sensitive to NO_2 at temperatures below 400 °C and to H_2 at temperatures above 400 °C. In addition, the response observed for the studied SiOCN ceramics is higher than that reported in the previous studies for SiOC ceramic aerogels. With regard to the optical gas sensing of the SiOCNs obtained from the heat treatment of the polymer precursors at 400 and 600 °C, fluorescence spectra in the presence of organic vapors such as acetone and hexane were recorded. The results show that these tested vapors quench the fluorescence of the studied SiOCN. In conclusion, the SiOCN ceramics can be promising materials for the gas sensing application.

Chapter 1 Introduction and literature review

1.1 Polymer derived ceramics (PDCs)

PDCs are ceramics obtained through a controlled pyrolysis process of polymer precursors.[1] This class of materials has gained much attention since several decades due to their advantages over traditional ceramics. For example, the characteristics of the final ceramics such as chemical composition, microstructure, crystallization behavior, electrical and optical properties can be tailored by controlling the chemistry of the polymer precursors and pyrolysis conditions (temperature, atmosphere, annealing time). Besides, PDCs can be produced without addition of sintering additives or flammable solvents which are usually needed for processing of traditional ceramics like powder technology.[1]

In the PDC field, organosilicon-based polymers are the most common precursors. A list of diverse Si-based polymer precursors is shown in Figure 1. By changing the atoms or/and functional groups surrounding Si, we can design the structure of polymer precursors in order to obtain the resultant ceramics with expected compositions and properties.
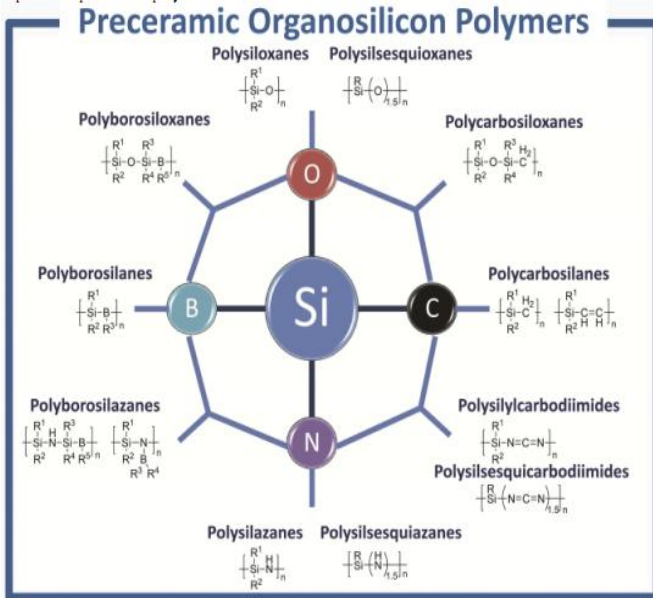
Figure 1: Main classes of Si-based polymer precursors.[1]

According to the number of elements present in the final ceramic, PDCs are basically divided into different subcategories such as binary systems (Si-C, Si-N), ternary systems (Si-O-C, Si-C-N), and quaternary systems (Si-B-C-N, Si-B-O-C). In addition to these common elements, other chemical components like Al, Ti, etc… can be possibly inserted into the polymer precursors. The corresponding ceramics obtained from different polymer precursors are shown in Figure 2.
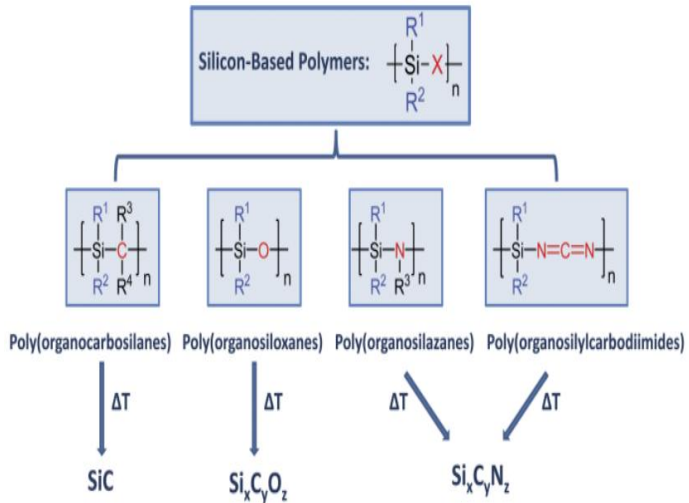
Figure 2: Thermal decomposition of Si-based polymer precursors.[1]

PDCs have shown exceptional properties such as high thermal stability, creep and oxidation resistance, and excellent chemical durability.[2-7] They also exhibit very interesting optical, electrical and electrochemical properties for potential functional applications.[8-10]

PDCs have found a wide range of potential applications such as micro-electro-mechanical systems (MEMS) for micro actuators, catalyst supports for fuel reforming, and anode materials in lithium ion batteries.[11-15]

1.2 Silicon oxycarbide (SiOC)

SiOC refers to a ceramic having chemical structure in which silicon is simultaneously bonded with carbon and oxygen atoms. The composition of the SiOC ceramics can be simply described as SiO_xC_{4-x}, $0 \leq x \leq 4$, which contain all possible Si sites as a mixture of SiC_4, $SiCO_3$, SiC_2O_2, $SiCO_3$ and SiO_4 units. The presence of tetrahedral units in the SiOC is supposed to be the reason for many of their excellent properties, compared to silicate glasses, such as higher glass transition temperature, higher elastic modulus and lower devitrification tendency.[7,16,17]

1.2.1 Synthesis methods

SiOCs can be produced through pyrolysis of preceramic polymer networks in inert atmospheres. These preceramic networks are obtained by: (i) sol-gel method using hybrid silicon alkoxides; (ii) hydrosilylation reaction using commercially available polysiloxanes; (iii) oxidation process of polycarbosilanes.[2,18,19]

1.2.1.1 Sol-gel method

The sol-gel process is a helpful technique to produce homogeneous SiOC glasses. One of the advantages of this method is that the synthesis might be performed at low temperatures. Carbon atoms are incorporated into the silica network using starting precursors of hybrid alkoxysilanes described as $R_xSi(OR')_{4-x}$; R= H, CH_3, C_2H_5, C_3H_7, C_2H_3, C_6H_5; R' = CH_3, C_2H_5. The nature of these alkyl groups, for instance, the number of carbon atoms, plays a key role in determining the chemical compositions and the properties of the resulting SiOC ceramics.[20] The precursor gels are obtained after hydrolysis and condensation reactions which do not

modify the carbon functional groups (R) in the starting silicon alkoxides. Thus, the obtained gels contain a mixture of Si-O and Si-C bonds which are simultaneously distributed, as shown in Figure 3.
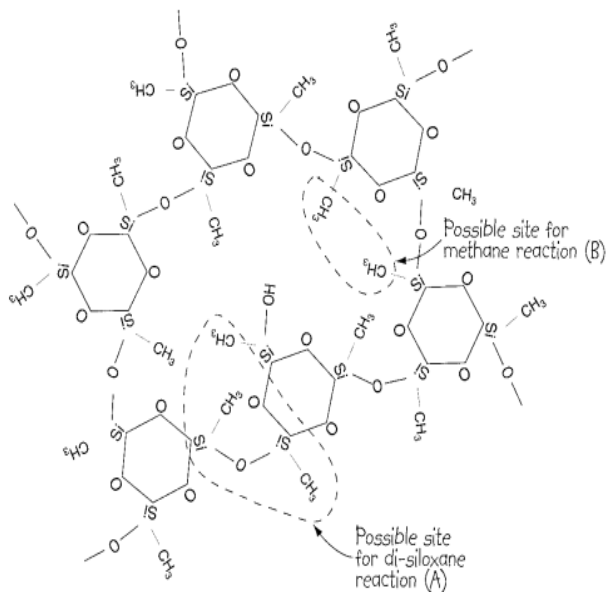
Figure 3: Structure of a preceramic polymer gel for SiOC.[20]

The main reactions taking place during the hydrolysis and condensation of the precursor gels are displayed in Scheme 1:
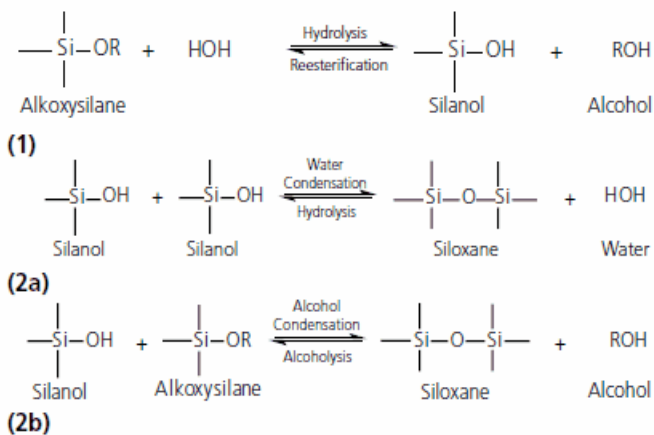
Scheme 1: Sol-gel reaction of alkoxysilane: (1) hydrolysis, (2a and 2b) condensation.[21]

1.2.1.2 Hydrosilylation

Hydrosilylation reaction is used to cross-link polysiloxanes containing Si-H bonds with cross-linkers having -HC=CH$_2$ groups. This reaction is achieved by either the addition of platinum-based catalyst or a free radical initiation technique.[19] This synthetic route allows us to easily tailor the structure of the preceramic precursor by changing the chemistry and amount of the vinyl bearing cross-linkers. The hydrosilylation mechanism is shown in Scheme 2.
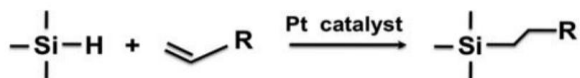
Scheme 2: Hydrosilylation reaction in the presence of Pt catalyst.[19]

1.2.1.3 Curing method

An alternative preparation method of SiOCs is to start from polycarbosilanes, precursors for SiC ceramics.[22,23] The oxygen incorporation into SiC networks occurs during a curing process. The oxidation mechanisms are shown in Scheme 3.
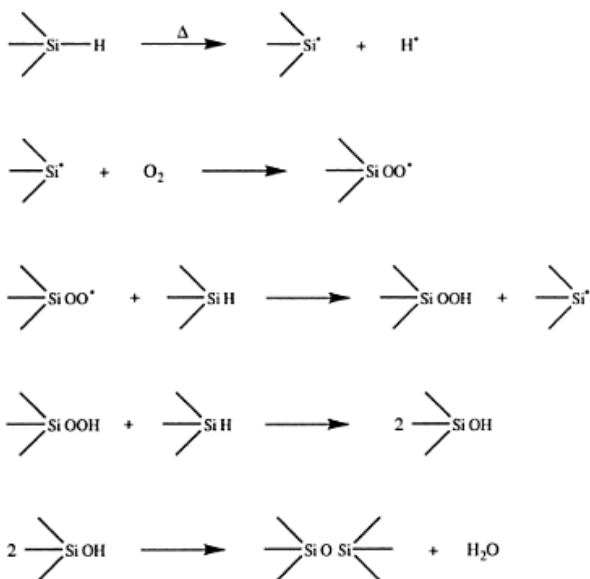
Scheme 3: Oxidation mechanism of a polycarbosilane.[24]

In comparison with the sol-gel method, the polycarbosilane-derived SiOCs contain a lower O and a higher C content.[22]

1.2.2 Structure of SiOCs

The compositions of SiOCs can be expressed as: $SiC_xO_{2(1-x)} + yC_{free}$; with $SiC_xO_{2(1-x)}$ is an amorphous network and C_{free} is a free carbon phase generated during pyrolysis at high temperature. The values of x and y can be controlled by the chemistry of the preceramic precursors and the pyrolysis conditions, in particular temperature and atmosphere. The importance of these factors is discussed in the following context.

First, the design of the precursors could lead to three different possibilities in the final ceramics: (i) the final ceramics without free carbon (y=0) are prepared using precursors containing together with Si-R (alkyl groups) also Si-H and Si-Si bonds;[25,26] (ii) SiOCs with a low amount of free carbon if Si is bonded to alkyl group such as CH_3. The longer carbon chain the precursor has, the higher content of carbon the resulting ceramic contains; (iii) SiOCs with a high content of free carbon are obtained from precursors having unsaturated groups such as vinyl and phenyl.

Second, the pyrolysis temperature significantly influences the structure of the resulting SiOCs. At temperatures below 1000 °C, amorphous SiOCs containing simultaneous Si-O and Si-C bonds are obtained. Between 1000 and 1400 °C, the amorphous network undergoes a phase separation resulting in the formation of nanostructural SiC-rich and SiO_2-rich regions, as illustrated in reaction 1:

$$SiOC \rightarrow a\text{-}SiO_2 + a\ SiC + C\ (1)$$
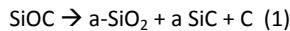
At temperatures above 1400 °C, the crystallization of SiC occurs and results in the formation of nanocrystals of SiC in the SiOC or silica network. At this temperature range, SiC crystallization takes place together with the carbothermal reactions and leads to the loss of carbon, as shown in the following equations:

11

$$SiO_{2(s)} + 3C_{(s)} = SiC_{(s)} + 2CO_{(g)} \quad (2)$$

$$2SiO_{2(g)} + SiC_{(s)} = 3SiO_{(g)} + CO_{(g)} \quad (3)$$
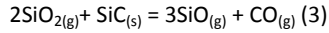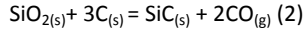
Third, the pyrolysis atmosphere has been shown to affect the final chemical composition of the SiOCs. For examples, the pyrolysis performed in hydrogen leads to a reduction in the amount of free carbon compared to that obtained in argon atmosphere.[27]

To have a better understanding of the unusual properties of the SiOCs, many structural models have been proposed. One of the very first structural models of amorphous SiOC glasses was proposed by Pantano *et al.*[20] According to his proposal, aromatic carbon species are either bonded to the oxycarbide network or embedded in the glass structure, as displayed in Figure 4.
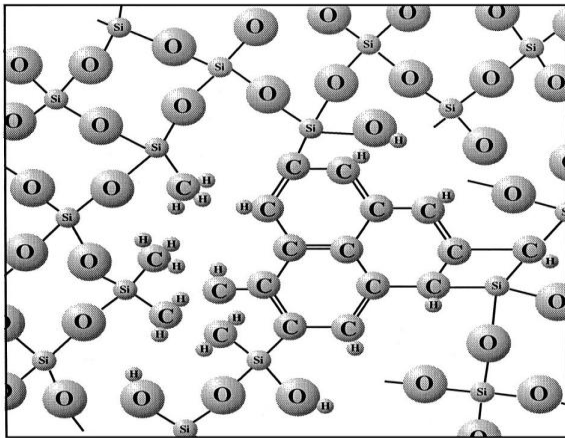
Figure 4: Schematic representation of an amorphous SiOC pyrolyzed at 800-1000 °C.[20]

Later on, Scarmi *et al* have proposed two possible models for the nanostructure of the amorphous SiOCs (Figure 5).[28] As shown in Figure 5a, nanodomains of sp^2 carbon discontinuously distribute in the silica matrix. On the other hand, second model (Figure 5b) shows a cage-like network of sp^2 graphene carbon in which silica domains are embedded together with the SiOC tetrahedra.
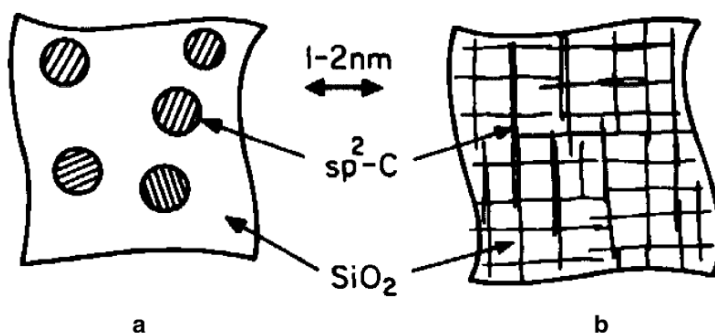
Figure 5: Two possible structure models of SiOCs (a) separate nanodomains of sp^2 carbon; (b) cage-like network of sp^2 graphene carbon.[28]

These models are likely to be contrary to each other. However, both of them are in agreement with the SAXS and NMR results in terms of the chemical structure.[29] In these proposed structures the mixed SiOC tetrahedral bonds locate at the interface between the nanodomains of sp^2 carbon and clusters of silica.

However, model A is not suitable for explaining several peculiar characteristics of the SiOCs. First, the continuous silica phase should lead to the formation of cristobalites at high temperature. Nevertheless, silica cristobalites indeed have not been observed in the SiOCs pyrolyzed even at

13

high temperatures. Second, the separate nanodomains of carbon should not suppress the viscosity of the silica phase that was experimentally observed in the SiOCs.[28] Third, by HF etching the silica phase we should produce C or SiC nanoparticles while it has been shown that a porous C-rich material is formed whose porosity matches exactly the volume of the initial silica phase.[30,31] In contrast with model A, model B can explain well for the creep and viscoelastic behavior that are ascribed to the graphene carbon network, and for the high crystallization resistance that are attributed to separate domains of silica.

In accordance with model B, Saha *et al* proposed a structure in which the existence of nanodomains in the SiOCs is incontrovertible.[29] During pyrolysis, carbon is ejected to the outer surface of the silica tetrahedra. Till these graphene-like carbons and mixed C-Si-O-bonds form a continuous path, nanodomains are accordingly created. As shown in Figure 6, the nanodomain model is constituted of clusters of silica, mixed bonds and graphene network. According to Saha *et al*, nanodomain size and the interdomain wall thickness (δw) can be possibly estimated.
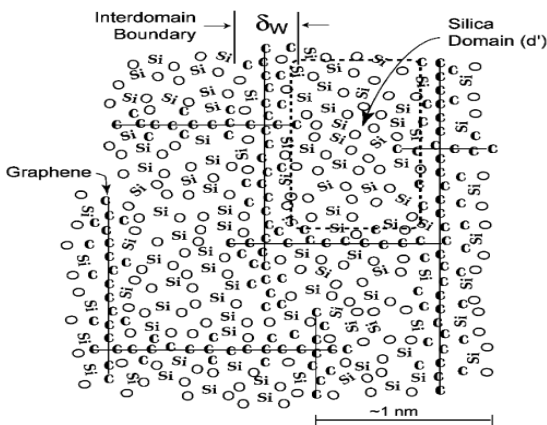
Figure 6: A nanodomain model of SiOCs.[29]

14

Later on, Widgeon *et al* have shown that silica-rich nanodomains in the structure of SiOCs are not only isolated but also interconnected, as displayed in Figure 7.[32]
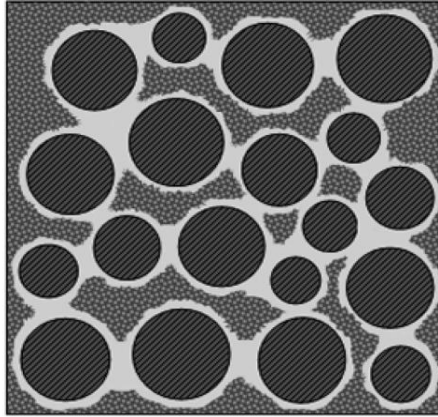
Figure 7: A nanoscale model of a SiOC pyrolyzed at 1100 °C: carbon nanodomains (dark shaded circles), C-rich SiOC region (light gray surrounding circles) and O-rich SiOC region (patterned matrix).[32]

1.2.3 Physical properties

Due to the main objective of this thesis, a review on the electrical, optical properties and application for gas sensing of the SiOCs will be discussed in the subsequent content.

1.2.3.1 Electrical property

The electrical conductivity of the SiOC ceramics varies in a wide range of 10^{-13} to 10^{0} (S.cm^{-1}).[33-35] This large variation of the electrical conductivity is caused by the difference in the pyrolysis temperature,

microstructure and carbon content. The pyrolysis temperature could be the most influent factor on the electrical conductivity since the change in carbon content and microstructure can be considered as its consequences. As seen in Figure 8, at low pyrolysis temperatures between 250 and 700 °C, both SiOCs derived from two polysilaxanes, namely PPS and PMS, are insulating materials. However, increasing pyrolysis temperature leads to a remarkable upgrade in the electrical conductivity which is in the semiconducting range.
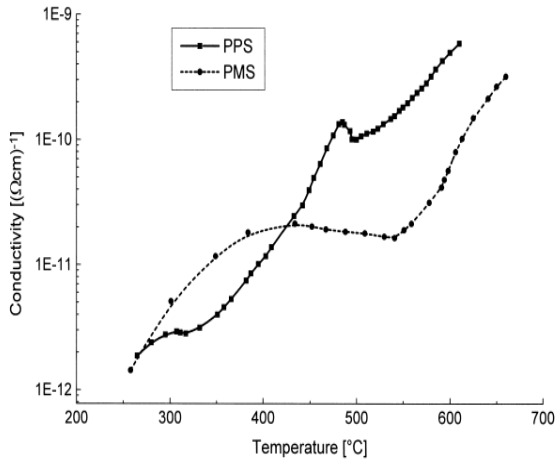
(a)
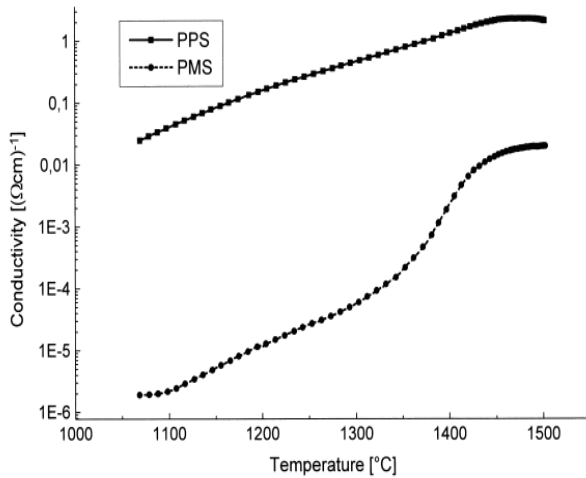
(b)

Figure 8: In situ electrical conductivity of SiOCs (a) from 250 to 700 °C; (b) from 1000 to 1500 °C. SiOC ceramics derived from two polysiloxanes, $(RSiO_{1.5})n$ with R = CH_3 (PMS) and C_6H_5 (PPS).[34]

Interestingly, the influence degree of the temperature on the conductivity between these two precursors is unsimilar. In details, the PPS-derived SiOCs show a slight raise of two orders of magnitude in conductivity with an increasing the pyrolysis from 1000 to 1500 °C. Unequally, the PMS-derived SiOCs exhibits a remarkable increase of four orders of magnitude in the conductivity in this temperature range. The reason could be that the PPS-derived ceramics contain a higher content of carbon and also this free carbon phase already forms a percolation network at 1000 °C while this process happens at higher temperature, ~ 1400 °C, for the PMS-derived samples. A model proposed by Engel *et al*, shown in Figure 9, helps us understand better why the pyrolysis temperature differently influences the conductivity.[34]
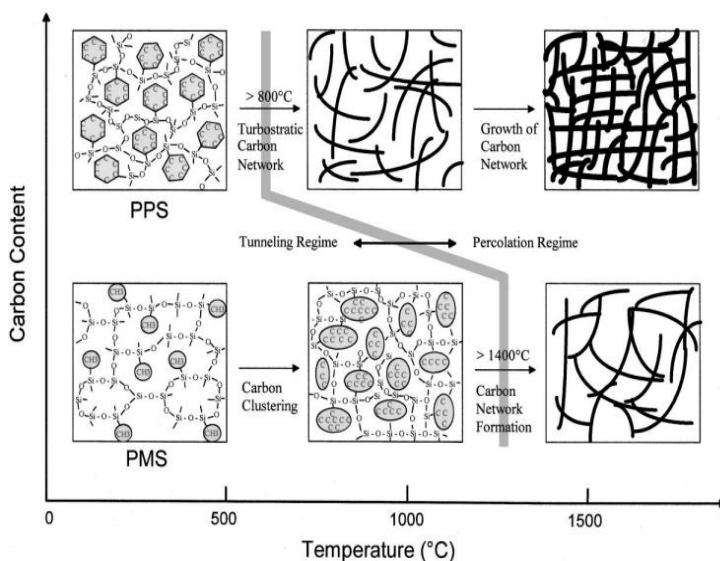
Figure 9: Redistribution of carbon during pyrolysis in the SiOCs derived from: (top) PPS, and (bottom) PMS.[34]

The above models show the growth of the carbon network with the pyrolysis temperature. However, the role of the amorphous SiOC microstructure on the electrical conductivity should not be underestimated because the amorphous SiOC network can become the main conducting phase depending on the pyrolysis temperature.[35]

1.2.3.2 Optical property

SiOC glasses are generally black because of the presence of layers of sp^2 carbon atoms in their structure. Thus, optical properties of these materials have not gained much attention. The effort of making transparent SiOC ceramics has been made.[25] Photoluminescence of different transparent SiOC glasses, so-called stoichiometric SiOCs, obtained from a triethoxysilane/methyldiethoxysilane sol-gel solution (TH/DH) shows a broad emission centered at about 500 nm which is ascribed to the presence of sp^2 carbon clusters.[36]

In 2009, Karakuscu *et al* successfully prepared SiOC thin films from a sol-gel solution mentioned above (TH/DH) with different ratios between TH and DH.[8] She found that amorphous SiOC thin films pyrolyzed at temperatures between 800 and 1000 °C show a blue luminescence, originated from dangling bonds, while those pyrolyzed at higher temperatures (≥ 1100 °C) show a green-yellow luminescence, due to the coexistence of both SiC and low amount of free carbon. Moreover, Si-rich SiOC thin film exhibits an intense white luminescence due to the simultaneous presence of SiC, C, and Si.

Recently, pyrolysis of silicon resin particles in H_2 atmosphere has been used to produce white SiOC ceramics.[37,38] The photoluminescence spectra of the white SiOCs pyrolyzed in the range of 800 and 1300 °C in

pure H_2 are shown in Figure 10. The photoluminescence is consistent with that obtained for the SiOC thin film. In details, SiOC powders pyrolyzed at 800 °C show a blue emission. The increasing of the pyrolysis temperature results in a slight red-shift and broader emission. The origin of luminescence might be correlated to the oxygen-defects generated during the pyrolysis process. This hypothesis agrees nicely with the results recently reported by Nikas *et al.*[39] Nikas and his colleagues believe that structural defects in oxides such as Si-related neutral oxygen vacancies and non-bridging oxygen hole centers are the main luminescence emitting centers.
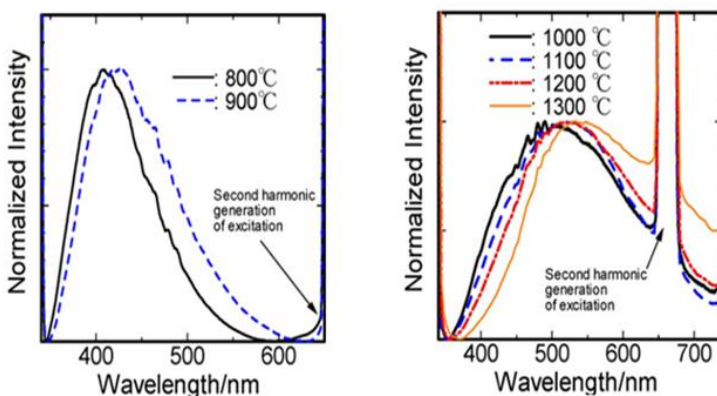
Figure 10: Photoluminescence spectra of white SiOC powders pyrolyed between 800 and 1300 °C.[38]

1.2.4 Gas sensing application

The possible use of SiOC for the detection of gas was reported for the first time by Karakuscu *et al* in 2013.[40] The gas sensing behavior was measured based on the variation of conductance of the SiOC powders in the presence of various gases. They observed that highly porous SiOC pyrolyzed at 1400 °C can be used to detect trace of NO_2 (5 ppm) at

temperatures below 400 °C. However, the SiOC loses its sensitivity to NO_2 at temperatures above 400 °C. On the contrary, the SiOC is sensitive to H_2 (2000 ppm) at temperatures above 400 °C and does not show any gas response below this temperature. Moreover, they also found that the studied SiOC is not sensitive to acetone and CO at any temperatures, as illustrated in Figure 11. However, the gas sensing mechanism is still an issue of debate.
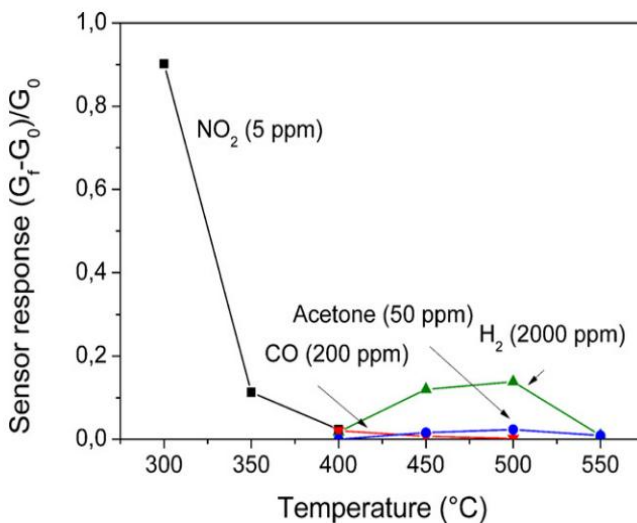
Figure 11: Gas response of a porous SiOC pyrolyzed at 1400 °C toward to NO_2, CO, H_2 and acetone.[40]

1.3 SiCN

SiCN ceramics are generally obtained via pyrolysis of either polysilazanes or polycarbodiimides. Besides these methods, SiCNs can be prepared using deposition techniques. In the following context, different

synthesis methods of the precursors, physical properties and gas sensing application of the SiCNs will be discussed.

1.3.1 Synthesis methods

1.3.1.1 Polysilazanes

Polysilazanes, one of the most popular precursors for SiCN ceramics, have been prepared via ammonolysis or aminolysis reaction of chlorosilanes, as shown in Scheme 4.[41-44]
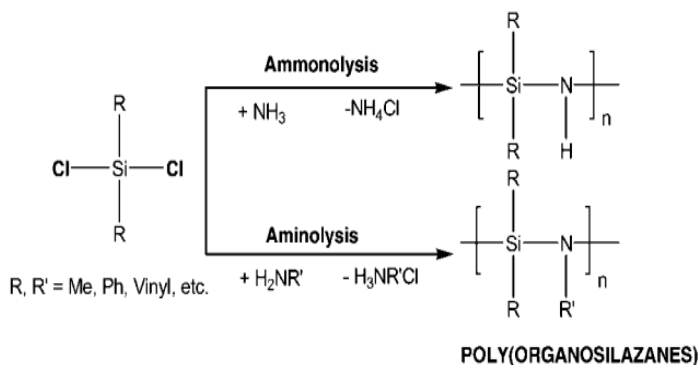
Scheme 4: Ammonolysis and aminolysis of chlorosilanes.[44]

Likewise SiOCs, properties of SiCN ceramics can be controlled by the chemistry of the substituted alkyl groups and pyrolysis conditions. As seen from Scheme 4, solid by-products such as NH_4Cl and $H_3NR'Cl$ are produced in these synthesis routes. As a result, the attained solid salts cause a difficulty in the separation and purification of the synthesized polysilazanes. To avoid this problem, dehydrocoupling reaction might be employed to prepare polysilazanes.[45,46] In this method, the use of a

transition metal as a catalyst is required. The reaction is shown in Scheme 5. However, handing hydridosilanes is more dangerous than chlorosilanes used in the ammonolysis and aminolysis reactions.

$$nR_2SiH_2 \ + \ nR'NH_2 \ \xrightarrow{\text{catalyst}} \ n/x[R_2SiNR']_x \ + \ 2nH_2$$
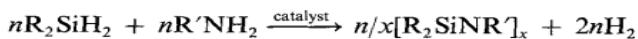
Scheme 5: Synthesis of polycarbosilazanes by dehydrocoupling reaction.[46]

1.3.1.2 Polycarbodiimides

Polysilylcarbodiimides were found as precursors for SiCN ceramics.[47,48] They can be synthesized from chlorosilanes and bis(trimethylsilyl)carbodiimides in the presence of pyridine used as a catalyst. The reaction is shown in Scheme 6.

Scheme 6: Carbodiimidolysis and cyanamidolysis of chlorosianes with bis(trimethylsilyl)carbodiimide and cyanamide.[36]

In terms of the mechanism, the carbodiimidolysis is similar to the sol-gel reaction of alkoxysilanes. A comparison between these two synthetic routes is shown in Figure 12. In comparison with the ammonolysis/aminolysis reaction, no solid salt is produced in the carbodiimidolysis.
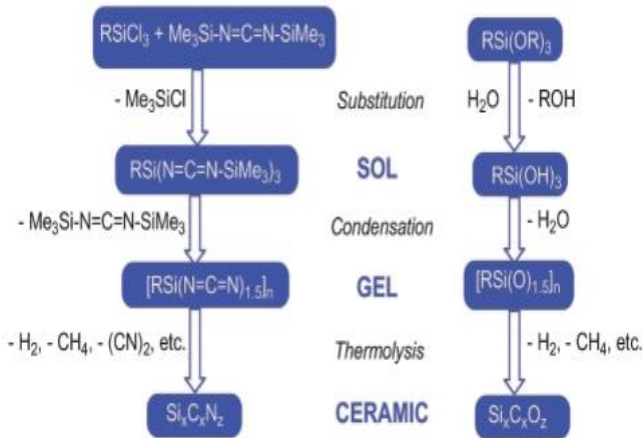
Figure 12: A comparison between the carbodiimidolysis and sol-gel reaction.[44]

1.3.2 Structure of SiCNs

Amorphous polysilazane-derived SiCN ceramics are constituted by a SiCN network and a free carbon phase.[9,49] The SiCN network contains tetrahedral mixed units SiC_xN_{4-x} ($1 \leq x \leq 4$) in which Si atoms are bonded to either N or C atoms.[50] A relative fraction of these mixed bonds is determined by the structure of the starting precursors. For example, methyl-bearing precursors result in the formation of an amorphous SiCN with a higher fraction of SiC_4 units whose chemical composition lies in the $C/SiC/Si_3N_4$ triangle while the vinyl-containing precursors lead to an amorphous SiCN constituted of mainly SiN_4 units whose chemical composition lies on the Si_3N_4-C tie line.[51] Ternary Si/C/N phase diagrams with the composition of the ceramics derived from these two precursors

are shown in Figure 13. At temperatures above 1438 °C, the decomposition process occurs according to reaction 4:

$$Si_3N_4 + C \rightarrow SiC + N_2 \text{ (4)}$$
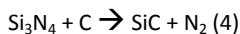
The final compositions of the ceramics derived from polyvinylsilazane and polyhidridomethylsilazane precursors, pyrolyzed at the temperature between 1438 and 1876 °C, could be C/SiC and SiC/Si$_3$N$_4$ composites, respectively.
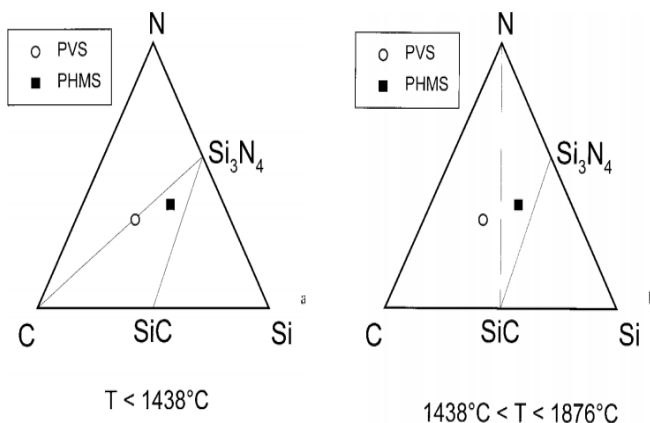
Figure 13: Ternary Si/C/N phase diagram and chemical compositions of the SiCN ceramics derived from polyvinylsilazane (PVS) and polyhidridomethylsilazane (PHMS).[51]

Amorphous polycarbodiimide-derived SiCN ceramics are composed of an amorphous Si$_3$N$_4$ and a carbon phase.[52,53] The presence of tetrahedral mixed bonds between Si and C/N is negligible. Structural characterization of the amorphous SiCN at the nanoscale shows that an interface made of mixed bonds N-Si-C is present in the SiCN containing a

25

low carbon content (39%) while these mixed bonds disappear in the system with a higher content of carbon, as shown in Figure 14.[54]
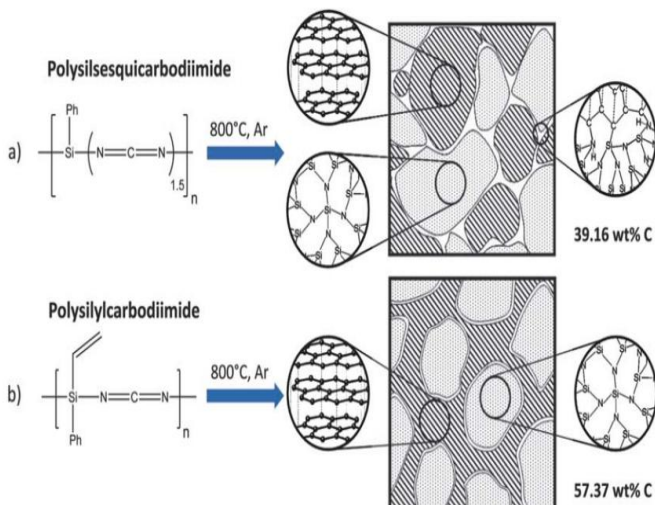
Figure 14: Nanodomain model of amorphous SiCNs obtained from different precursors: (a)Polysilesquicarbodiimide, (b) Polysilylcarbodiimide.[54]

Mera and her colleagues also found that increasing pyrolysis temperature up to 1100 °C results in an amorphous SiCN without mixed bonds, as shown in Figure 15.
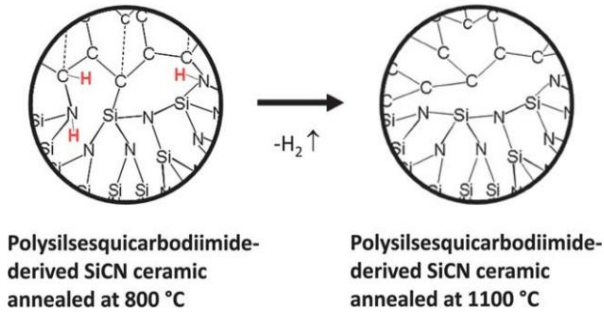
Figure 15: The loss of H and the mixed bonds caused by an increase of the pyrolysis temperature.[54]

1.3.3 Physical properties

1.3.3.1 Electrical property

Electrical conductivity of SiCN strongly depends on its microstructure and chemical compositions which are very sensitive to the pyrolysis conditions, as shown in Figure 16.[9,55,56] At low temperature regime ranging from 1000 to 1400 °C, an increase of electrical conductivity is ascribed to an increase of sp^2/sp^3 ratio of carbon atoms. In the higher temperature regime between 1400 and 1600 °C, nano-crystallites of SiC are generated and they are responsible for the increase of electrical conductivity. At temperature above 1600 °C, SiCN is constituted by crystallites of SiC and Si_3N_4 in which SiC becomes the main conducting phase.[55] However, the identification of the conduction mechanism in SiCN is still controversial. Trassl and his groups believe that the conductivity of SiCN is correlated to the ordering degree and the amount of free carbon phase.[9,56]
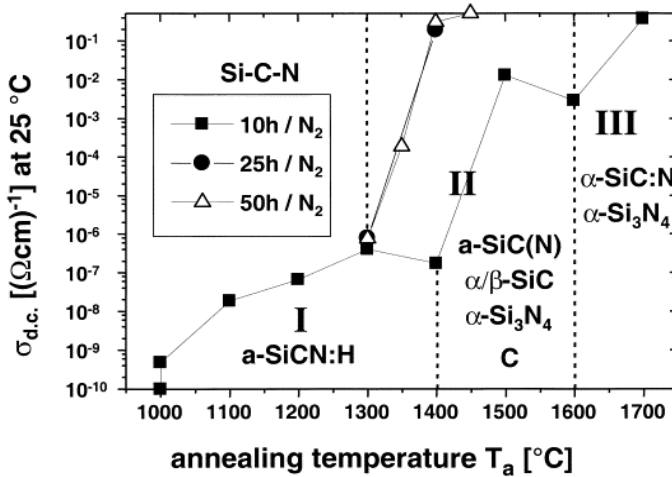
Figure 16: Electrical conductivity of SiCN ceramics as a function of annealing time and temperature.[55]

1.3.3.2 Optical property

In 2008, Menapace *et al* reported the possible applicability of thermally treated polysilazanes as LEDs.[57] She pointed out that a commercial poly(ureamethylvinyl)silazane heated at low temperatures between 200 and 600 °C exhibits photoluminescence, as shown in Figure 17.[57] An increase of the heating temperature causes a red-shift in excitation and emission spectra of the materials. Also, fluorescence intensity depends on the treatment temperature. The sample heated at 500 °C is discovered to be an interesting material for LED application because it is transparent and shows photoluminescence in the visible range with a maximum blue emission. The origin of luminescence is associated with the formation of dangling bonds and sp^2 carbon formed during the heat treatment.

28
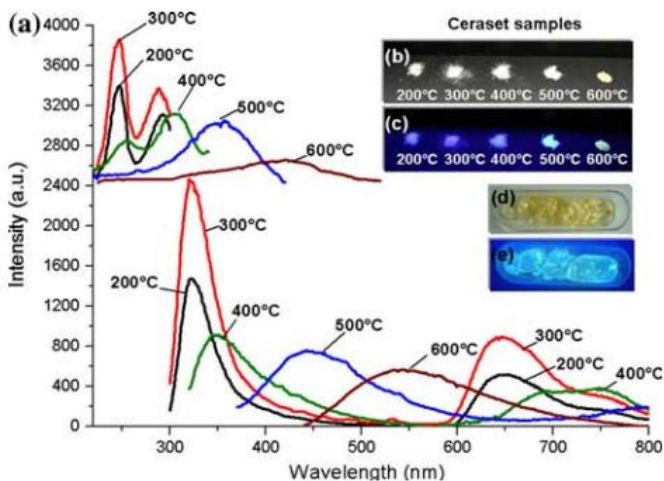
Figure 17: Fluorescence properties of Ceraset samples heat-treated at different temperatures: (a) Emission (bottom right) and excitation spectra (top left), (b) Photographs representing powdered Ceraset samples under white light, (c) Photographs representing powdered Ceraset samples under UV light, (d) Photographs representing Ceraset annealed at 500 °C under white light,(e) Photographs representing Ceraset annealed at 500 °C under UV light.[57]

Recently, Mera and her groups have investigated the photoluminescence of a variety of phenyl-containing polycarbodiimides heated at low temperatures.[58] These studies indicate that apart from the free carbon, crosslinking degree of the polymers is also responsible for the luminescence of the treated polymers.

1.3.4 Gas sensing application

To the best of my knowledge, no investigation on the gas sensing application of SiCN was reported in the literature. Recently, it has been discovered in our group that SiCN aerogels heated at 450 °C can be a promising material for the detection of organic solvents such as acetone and hexane.[59] It is clearly seen that the presence of organic vapors leads to an enhancement of the fluorescence compared to that recorded in N_2 atmosphere, as shown in Figure 18. Interestingly, fluorescence intensity is not influenced by water vapor. These findings suggest that the aerogel surface and/or the luminescence centers might have a strong hydrophobic character which is supposed to be correlated to the sp^2 carbon or aromatic compounds.[57,58] The increase of emission intensity can be due to the changes in the local environment of the molecules which give fluorescence. The adsorbed organic solvents can solvate and dissociate the fluorescence compounds from the aggregated ones.[60] As a consequence, the intermolecular vibronic interactions which induce the nonradioactive relaxation process are weakened.[61]
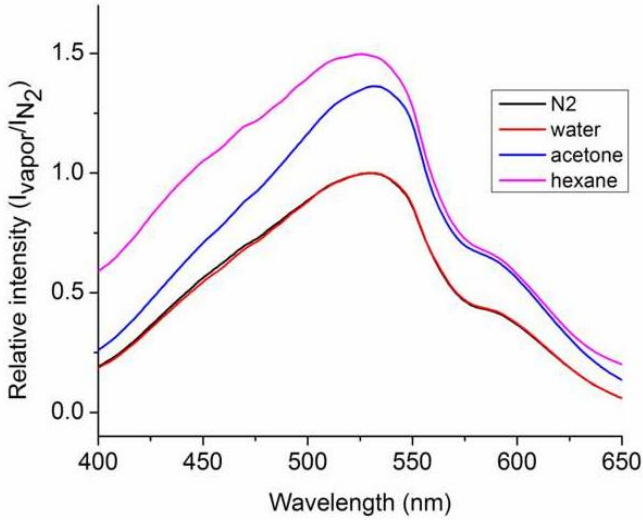
Figure 18: Emission spectra of a SiCN aerogel heated at 450 °C in different saturated vapors.[59]

1.4 SiOCN

Ternary SiOCs and SiCNs can be doped with extra elements to further extend the range of their interesting functional properties. In particular B-doping, resulting into Si(B)OC and Si(B)CN systems, have been extensively reported in the literature.[62-67] Boron atoms are present either in the amorphous SiOC network as $BC_{3-y}O_y$ units ($0 \leq y \leq 3$) or in the sp^2 C layers of the free C phase as substitutional BC_3 units in the Si(B)OC ceramics.[63,64] Whereas, B atoms are present in the BNC layer in the Si(B)CN ceramics.[67,68] Adding B into SiCN network could form a material that is stable up to 2000 °C.[65] The presence of B in the SiOC or SiCN matrix, however, reduces thermodynamic stability of the resulting

quaternary systems.[69,70] B-containing SiOCs exhibit a broader tunable emission in the visible range[71] and a higher electrical resistance [72], compared to B-free SiOCs. The presence of B, particularly in the B-C bonds, in the SiOC network could retard either the formation of C radicals, photoluminescence emitting centers, or the separation of free carbon, a conducting phase in the PDCs. As a consequence, the insertion of B atoms into the SiOC matrix significantly changes the electrical and/or optical properties of the corresponding PDCs. The influence of an extra element on the properties of the ternary PDCs is brought into question. What will characteristics of the SiOCs change if N is added into the network? In the literature, several studies focusing on the synthesis and characterization of SiOCN systems have been reported.[73,74]

SiOCN ceramics can be obtained via pyrolysis of the polymer precursors which are generally prepared from two main synthetic routes. The first method is the controlled incorporation of either N into polysiloxane or O into polysilazane obtained through a molecular approach. [73-75] This synthetic route allows us to control the chemical composition of the final SiOCN ceramic by the design of the chemistry of the starting materials. The second method is that oxygen is incorporated into the polysilazane from external source such as pyrolysis atmosphere. [76,77] The presence of O in the resulting SiOCN ceramics is caused by the oxidation reaction of Si-H/Si-C bonds.[78] One of the drawbacks of this method is the difficulty in controlling the chemical composition of the ceramics.

SiOCN is constituted by the mixed tetrahedral bonds between Si and the other elements, as shown in Scheme 7. Thermodynamic stability of SiOCN is shown to be dependent on the molar ratio of N and O.[79] The presence of both N and O in the SiOCN ceramic results in a more stable system compared to the ternary SiOC or SiCN ceramics evidenced by a lower formation enthalpy. However, this fact is not true for the SiOCN with

32

a ratio of N/O ~ 2 which shows a positive enthalpy of formation. The reason could be due to the formation of nanoclusters of Si_2N_2O in the amorphous matrix.
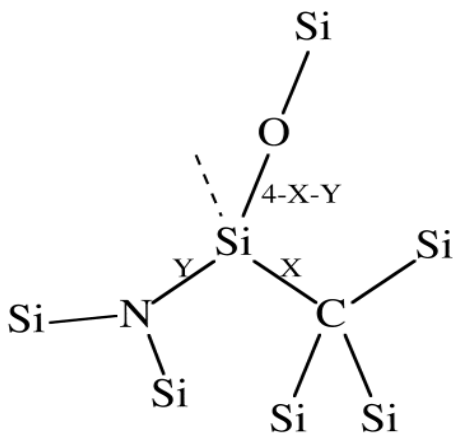
Scheme 7: Representation of tetrahedral bonds in $SiC_xN_yO_{4-x-y}$
$(0{\leq}x{\leq}x+y{\leq}4)$.[76]

Several properties of the SiOCN such as optical, oxidation and mechanical properties have been reported.[76,80,81] The SiOCN heated at low temperatures show an intense and a broad photoluminescence, in the visible range between 500 and 800 nm, which is strongly dependent on the composition and treated temperature.[81] According to Chollon, oxidation behavior of the SiOCN is governed by the C/Si and N/Si ratio. Interestingly, oxygen and free carbon do not play an important role on the oxidation mechanism.[76] On the contrary, free carbon phase is believed to be responsible for the low elastic modulus of the SiOCN.[80] However, all these studies have been done for the SiOCN obtained through uncontrolled incorporation of O into SiCN. Therefore, there is a need to systematically study the SiOCN obtained under controlled conditions.

33

Chapter 2 Experimental: Synthesis and Characterization Techniques

2.1 Synthesis of SiOCN ceramics

2.1.1 Chemicals

Polyhydridomethylsiloxane (PHMS) was supplied from Alfa Aesar, Italy. Platinum(0)-1,3-divinyl-1,1,3,3-tetramethyldisiloxane complex solution in xylene (Pt-based catalyst), 2,4,6-trimethyl-2,4,6-trivinylcyclotrisilazane (TMTVSLZ), triallylamine (TA) and 1,3,5-triallyl-1,3,5-triazine-2,4,6(1H,3H,5H)-trione (TTT) were purchased from Sigma-Aldrich, Italy. All the starting materials were used as received without further purification.

2.1.2 Synthesis of polymer precursors

PHMS/TMTVSLZ was prepared from a mixture of PHMS and TMTVSLZ in the presence of Pt-based catalyst (1 wt-% with respect to PHMS). This reaction was carried out at room temperature for 24 h and it was subsequently aged at 80 °C for 7 days to form a hard gel. PHMS/TA precursor was synthesized via the reaction of PHMS and TA at 0 °C for 24 h and subsequently it was aged at 80 °C for 7 days to obtain a hard gel. PHMS/TTT precursor was synthesized from a mixture of PHMS and TTT in cyclohexane at 70 °C under reflux conditions for 24 h. After a complete evaporation of the solvent, the cross-linked gel was aged at 90 °C for 7 days. The crosslinking mechanism of these three reactions is based on the hydrosilylation reaction between the Si-H groups of PHMS and the -CH=CH$_2$ functional groups in the reactants. The molar ratio between Si-H and -CH=CH$_2$ was kept unchanged (2:1) in all the syntheses. The average molecular weight of PHMS (1900 g/mol) was used to calculate the molar

34

ratio taking into account the presence, in the polymer structure, of the two $(CH_3)_3SiO$ terminal units. The manipulation of the reagents is performed under argon flow to prevent excessive interactions with air and moisture. All the reactions were carried out in air. The nominal compositions of the starting precursors are listed in Table 1.

Table 1: Nominal composition of the starting precursors

Precursor	Mass (g)	Expected formula of the precursor
PHMS/TMTVSLZ	10:6.8	$Si_3C_{5.3}O_{1.9}NH_{15.9}$
PHMS/TA	10:3.5	$Si_{9.5}C_{16.2}O_6NH_{42.8}$
PHMS/TTT	10:6.4	$Si_{2.1}C_{6.4}O_3NH_{14.2}$

2.1.3 Pyrolysis

An alumina tubular furnace was employed for the pyrolysis of the as-obtained gels. Fragments of the pre-ceramic polymers were placed in an alumina boat and were consequently inserted into the furnace for heat treatment. The SiOCN ceramic samples were produced by pyrolysis of the as-obtained gels for 1 h under flowing nitrogen (100 ml/min) at the desired temperature. The pyrolysis temperature was programmed with a heating rate of 10 °C/min and 10 °C/min cooling rate to room temperature. The final ceramics were then milled in an agata mortar to obtain fine powders.

2.2 Structural characterization

2.2.1 FT-IR

FT-IR spectra were collected on a Nicolet Avatar 330 Fourier transform infrared spectrometer (Thermo Electron Corporation, Waltham, MA) using KBr technique in transmission mode. An average of 64 scans with 4 cm^{-1} resolution was recorded for each specimen.

2.2.2 MAS NMR

The ^{13}C- and ^{29}Si- MAS NMR spectra of the synthesized polymer precursors were collected using an AVANCE300 Bruker 7 mm probe-head (Bruker, Instruments, Karlsruhe, Germany) operating at the frequencies of 59.62 and 75.48 MHz, respectively. All the ^{29}Si single pulse NMR spectra were recorded using a π/2 pulse length of 2.8 μs and a recycle delay of 300s. For the ^{13}C-NMR, single pulse experiments were performed using a π/2 pulse length of 2.2 μs and a recycle delay of 10 s.

The ^{29}Si-NMR experiments of the ceramic samples, pyrolyzed at 1400 °C were carried out using an AVANCE 400 Bruker 7 mm probe-head(Bruker, Instruments, Karlsruhe, Germany) operating at the frequencies of 79.49 MHz. The ^{29}Si single pulse NMR spectra were recorded using a π/4 pulse length of 2 μs and a recycle delay of 100s.

Polymer and ceramic samples were packed in 4 mm zirconia rotors which were spun at a rate of 7 and 8 kHz, respectively, under air flow. Q8M8, adamantine and ethanol were used as external secondary reference for the determination of the ^{29}Si and ^{13}C chemical shift.

2.2.3 TGA

TGA of the synthesized polymers were performed on a Netzsch apparatus (Model STA 409, Netzsch-Geratebau GmbH, Germany). The samples were heated to 1500 °C at a rate of 10 °C/min in nitrogen atmosphere with a flux of 100 mL/min.

2.2.4 XRD

XRD spectra of powdered ceramic samples that were pyrolyzed at different temperatures were recorded using a diffractometer (Model D-Max B, Rigaku, Tokyo, Japan) operated at 40kV and 30 mA with a CuKα radiation. The spectra were collected in the 2θ range of 20-80, with a step of 0.05° every 6 s.

2.2.5 Chemical analysis

The carbon content of the powdered ceramic samples was determined by a carbon analyzer (Leco TC-200, Leco Corp USA). The oxygen and nitrogen content were measured by an analyzer (Leco TC-436, Leco Corp USA).

2.2.6 XPS

XPS spectra of the powdered ceramic samples were recorded using a Science-ESCA 200 equipped with a hemispherical analyzer and a monochromatic Al Kα X-ray source. The corelines (C1s, N1s) were acquired at a pass energy of 150 eV. A Shirley-type background subtraction was applied. The spectra were fitted using a non-linear least-squares fitting program. The C1s core line with the main peak at 285 eV corresponding to amorphous carbon was used as internal reference to calibrate the spectra.

2.2.7 Raman

Raman spectra of the ceramic powders were recorded on a micro-Raman spectrometer (LabRAMAramis, Horiba JobinYvon, USA) by using a laser beam with an excitation wavelength of 532 nm.

2.2.8 SEM

The microstructure of the ceramic powders was studied using Jeol-JSM-5500 Scanning Electron Microscopy

2.3 Physical characterization

2.3.1 Impedance spectroscopy

Impedance spectroscopy (AutoLab Electrochemical Potentiostat PGSTAT 302N) was applied to measure electrical conductivity of SiOCN ceramic powders. The frequency tested was in the range of 10-10^6Hz, the applied voltage was 5 mV recording five experimental data points for each decade

2.3.2 Fluorescence measurement

Fluorescence spectra of the studied samples in air were obtained using spectrometer (Jasco FP6300) with a bandwidth of 5 nm, scanning rate of 500 nm/min. An excitation wavelength of 340 nm was used and the emission spectra were recorded with a CCD-detector in the wavelength ranging from 360 to 600 nm.

Chapter 3 N-doped SiOC ceramics from preceramic polymers: the role of the N-containing precursor

3.1 Introduction

The objective of this chapter is to synthesize N-doped SiOC ceramics using different N-containing precursors and then to characterize their structure and high temperature behavior, in particular the thermal stability and crystallization behavior. Accordingly, the influence of the molecular structure of the precursors on both the nitrogen content and its chemical bonding nature in the final ceramics has been investigated.

In this chapter, three different pre-ceramic polymer precursors for SiOCN ceramics are studied. The polymer precursors are synthesized via the hydrosilylation reaction between a linear polysiloxane containing Si-CH$_3$ and Si-H bonds, namely polyhydridomethylsiloxane, PHMS (HCH$_3$Si-O)$_n$, and vinyl-bearing organic compounds such as 2,4,6-trimethyl-2,4,6-trivinylcyclotrisilazane (TMTVSLZ), triallylamine (TA) and 1,3,5-triallyl-1,3,5-triazine-2,4,6(1H,3H,5H)-trione (TTT), with a constant molar ratio (2:1) of Si-H : -CH=CH$_2$ groups. Molecular structures of the starting materials are shown in Scheme 8.
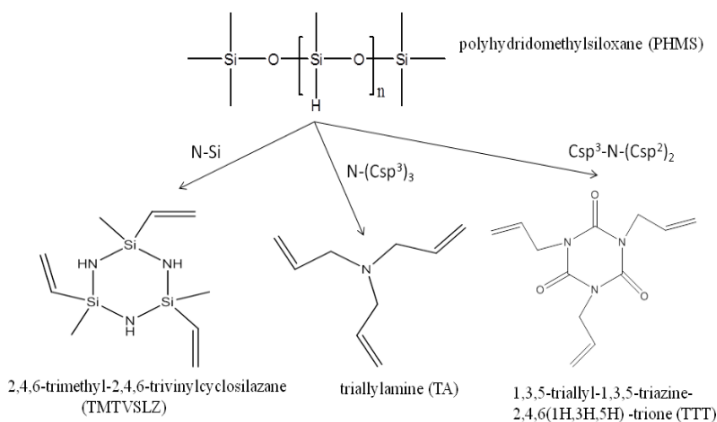
Scheme 8: Molecular structures of the starting materials.

40

It should be mentioned that N atoms in the starting materials exist in different chemical sites, for example in H**N**Si$_2$ units (TMTVSLZ), in **N**(C$_{sp}^3$)$_3$ (TA) and in **N**C$_{sp}^3$(C$_{sp}^2$)$_2$ units (TTT). The structural characterization of the as-synthesized precursors was performed by FT-IR, ^{13}C-NMR and ^{29}Si - NMR. Thermogravimetric analysis (TGA) was carried out to study the thermal stability of the synthesized polymer precursors. All the as-synthesized polymers were pyrolyzed at different temperatures varying between 800 and 1500 °C leading to the formation of the corresponding SiOCN ceramics. The chemical composition of the SiOCN ceramics was analyzed by elemental analysis. Furthermore, the structural evolution occurring between 1000 and 1500 °C was investigated by FT-IR, XRD and ^{29}Si-NMR. X-ray photoelectron spectroscopy (XPS) was employed to study the local chemical environment on different elements in the ceramics derived from PHMS/TMTVSLZ and from PHMS/TTT at 1000 °C.

3.2 Experimental

The polymer precursors were synthesized as reported in chapter 2. The ceramic samples were obtained through pyrolysis at 800, 1000, 1200, 1400 and 1500 °C.

3. 3 Results and discussion

3.3.1 Characterization of the pre-ceramic polymer precursors

3.3.1.1 FT-IR
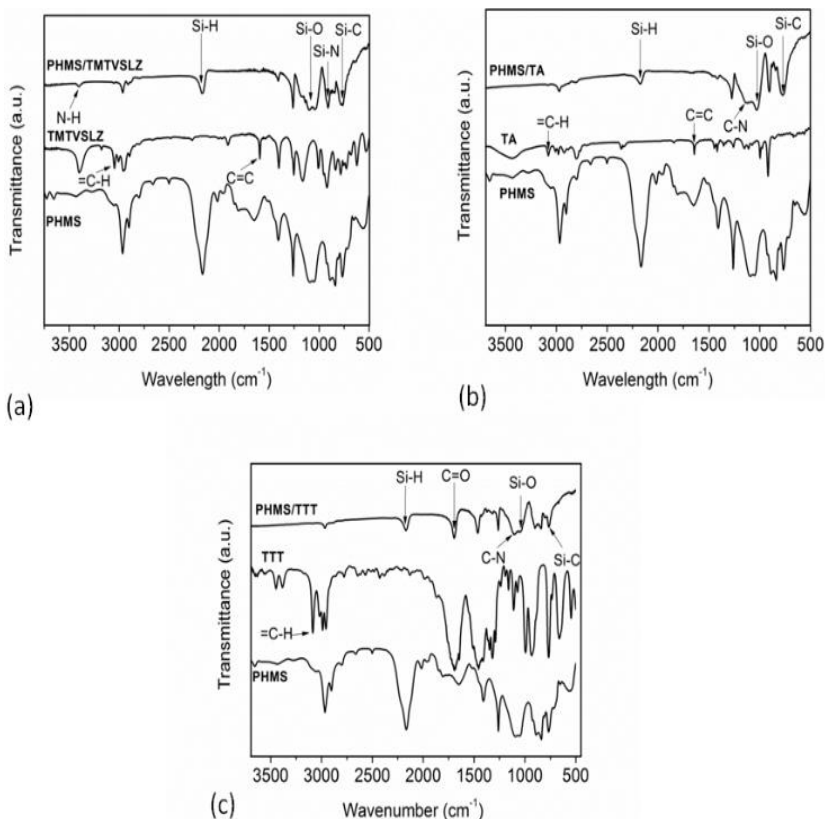
Figure 19: FT-IR spectra of the pre-ceramic polymer precursors (a) PHMS/TMTVSLZ, (b) PHMS/TA, and (c) PHMS/TTT. The FT-IR spectra of the PHMS and the N-containing compounds are also shown.

The FT-IR spectra of the as-synthesized pre-ceramic polymer precursors and the corresponding precursors (PHMS and N-containing compounds) are shown in Figure 19 and the main absorption bands of the spectra are listed in Table 2. In the case of the PHMS/TMTVSLZ precursor (Figure 19a), the FT-IR spectrum shows the presence of Si-O (1090 cm^{-1}), Si-N (922 cm^{-1}), Si-C (770 cm^{-1}), and N-H (3405 cm^{-1}) peaks confirming the combination of the polysiloxane and the silazane units in the starting materials. In the PHMS/TA precursor (Figure 19b), the simultaneous presence of Si-C, Si-O and N-C (1141 cm^{-1}) peaks shows the combination between PHMS and TA. For the PHMS/TTT precursor (Figure 19c), the spectrum shows absorptions of Si-O, C=O (1697 cm^{-1}) and N-C (1109 cm^{-1}) peaks due to the incorporation of TTT into the polysiloxane matrix. In all the FT-IR spectra, the disappearance of vinyl groups (H-Csp^2 peak at 3053 cm^{-1} and C=C peak at 1596 cm^{-1}) and a considerable decrease in the intensity of Si-H peak at 2168 cm^{-1} suggest the occurrence of the hydrosilylation reaction.

Table 2: Main FT-IR absorptions of the three as-synthesized polymer precursors.

Wavenumber (cm^{-1})	Assignments [73,82]
3394	νN–H (stretching)
3076, 3007	νCsp^2–H (stretching)
2975, 2900	νCsp^3–H (stretching)
2160	νSi–H (stretching)
1690	νC=O (stretching)
1643, 1591	νC=C (stretching)
1405	δC–H (CH$_3$ deformation)
1253	δC–H (Si-CH$_3$ deformation)
1134, 1105	νC–N (stretching)
1080	νSi–O–Si (stretching)
922	νSi–N–Si (stretching)
765	δSi–C (deformation)

3.3.1.2 NMR

(a)

(b)
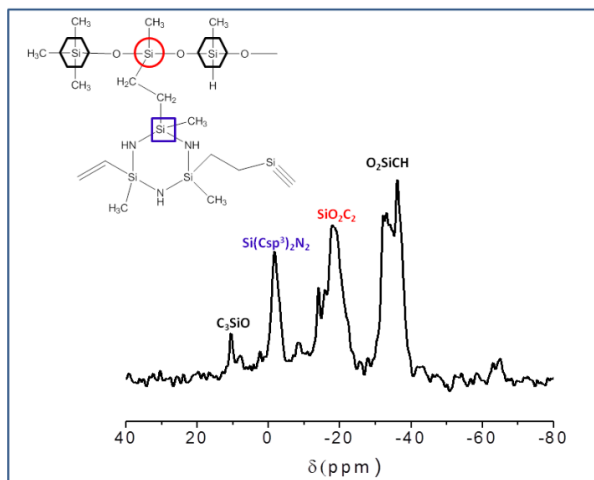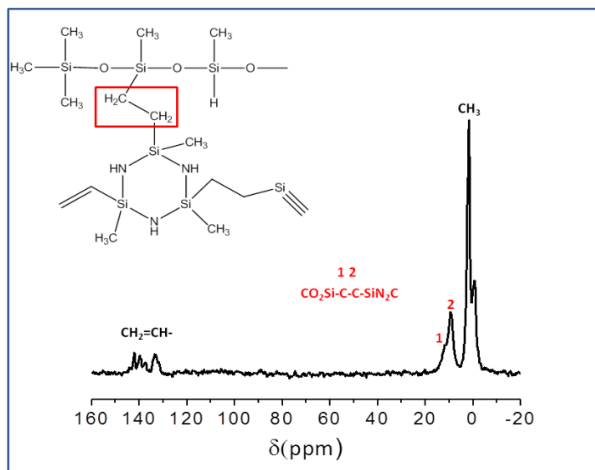
Figure 20: (a) ^{13}C- and (b) ^{29}Si-NMR spectra of the PHMS/TMTVSLZ precursor.

Figure 20 shows the spectra recorded on the PHMS/TMTVSLZ sample. The ^{13}C-NMR spectrum (Figure 20a) shows the peaks at ~ 0 ppm, due to the CH_3 groups in the starting PHMS and TMTVSLZ, and the peaks at 133.1 and 139.9 ppm, due to residual vinyl groups in the TMTVSLZ. More importantly, carbon atoms belonging to the CH_2 groups of the new Si-CH_2-CH_2-Si bridge formed through the hydrosilylation reactions give rise to the peak at δ =9 ppm with a shoulder at δ = 9.5 ppm.[50,83]

The ^{29}Si-NMR spectrum (Figure 20b) shows the peaks due to the Si sites in the precursors at the chemical shifts of -35.8 ppm (O_2SiCH) and 10.7 ppm (C_3SiO).[84] The spectrum also contains two new peaks at the chemical shifts of δ= -17.9 ppm and δ= -1.6 ppm which can be assigned to SiO_2C_2 [84] and $Si(Csp^3)_2N_2$, respectively.[50,85] These two new peaks result from the hydrosilylation reaction that was previously revealed by the ^{13}C-NMR spectrum.
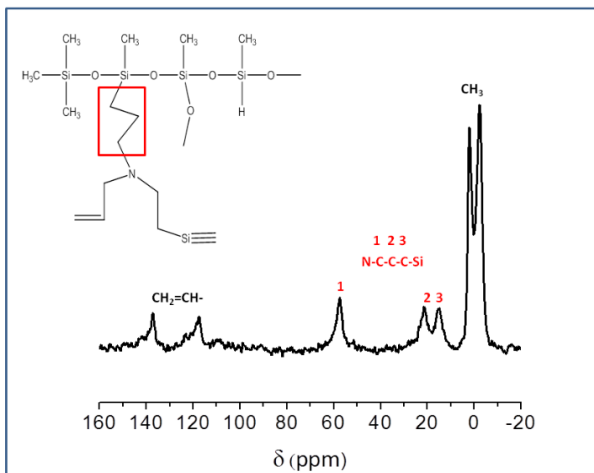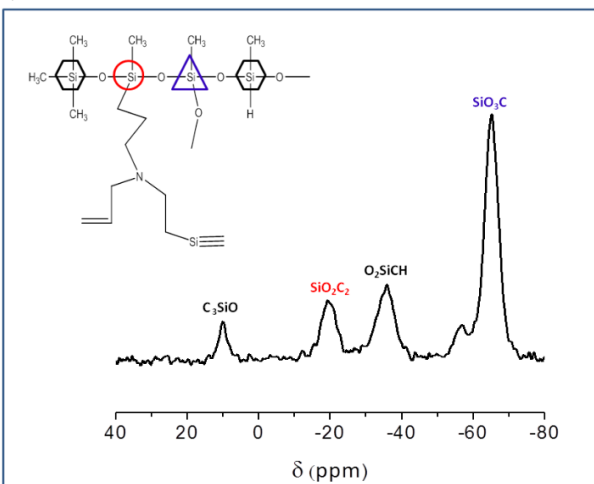
Figure 21: (a) ^{13}C- and (b) ^{29}Si-NMR spectra of the PHMS/TA precursor.

47

Figure 21 shows the spectra recorded on the PHMS/TA sample. The ^{13}C-NMR spectrum (Figure 21a) shows the peaks at the chemical shifts of -2.4 ppm and 1.9 ppm which are characteristics of the CH_3 units in the starting precursors.[84] The spectrum also displays the peaks at 117.6 and 137.4 ppm, corresponding to the residual vinyl groups in the TA. Especially, the spectrum shows three methylene carbon signals (δ = 15.2; 21.5 and 57.3 ppm) which suggest the formation of the Si-C-C-C-N bridge via the hydrosilylation reaction.[83,86] The ^{29}Si-NMR spectrum (Figure 21b) shows the Si units in the starting precursor at the chemical shifts of -35.6 ppm (O_2SiCH) and 10.1 ppm (C_3SiO). The spectrum also indicates two Si signals which belong to SiO_2C_2 units (δ= -19.2 ppm) and SiO_3C units (δ=-64.9 ppm).[84] The presence of SiO_3C units results from the hydrolysis of Si-H bonds with the moisture from the atmosphere.
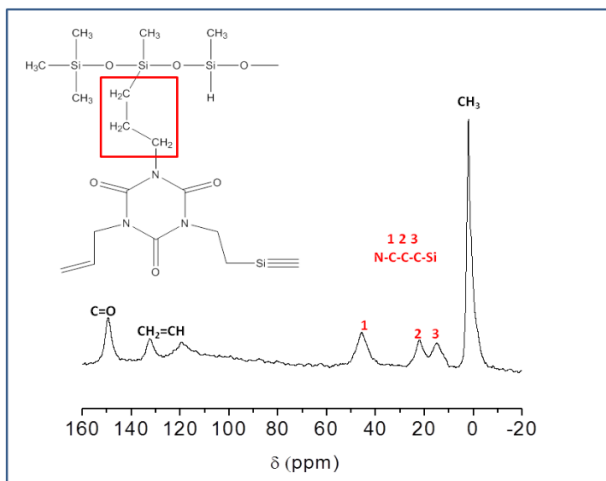
(a)
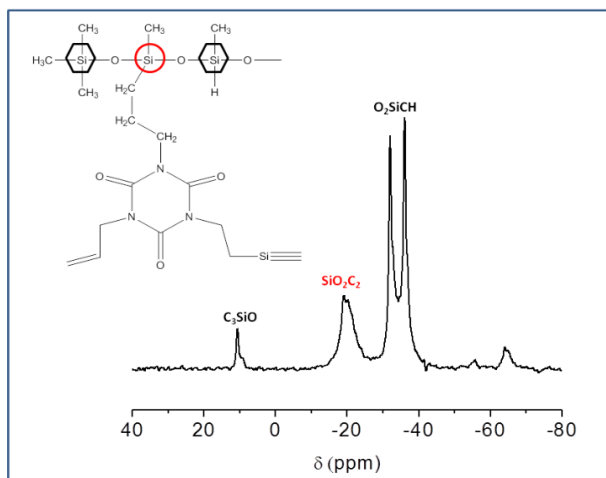
(b)

Figure 22: (a) ^{13}C- and (b) ^{29}Si-NMR spectra of the PHMS/TTT precursor.

49

Figure 22 shows the spectra recorded on the PHMS/TTT sample. The ^{13}C-NMR spectrum (Figure 22a) shows the peak at 149.5 ppm due to the C=O bonds, the peaks at 132.7 and 119.4 ppm due to the vinyl groups and the peak at 2.4 ppm due to CH_3 units which are retained from the precursor.[87] Besides, the spectrum displays three peaks at the chemical shifts of δ = 14.9; 21.57 and 45.9 ppm which are indicative of the three new methylene carbons formed through the hydrosilylation reaction. The ^{29}Si-NMR spectrum (Figure 22b) shows not only the Si peaks in the precursor, -36.2 ppm (O_2SiCH) and 10.4 ppm (C_3SiO) but also the new SiO_2C_2 units at the chemical shift of δ = -19.4 ppm. The ^{29}Si-NMR data are consistent with the ^{13}C-NMR data confirming the occurrence of the hydrosilylation reaction.

It should be pointed out here that the ^{13}C-NMR spectra of all the three as-synthesized precursors show residual vinyl groups because of steric hindrance resulting in an incomplete hydrosilylation reaction.

3.3.1.3 TGA
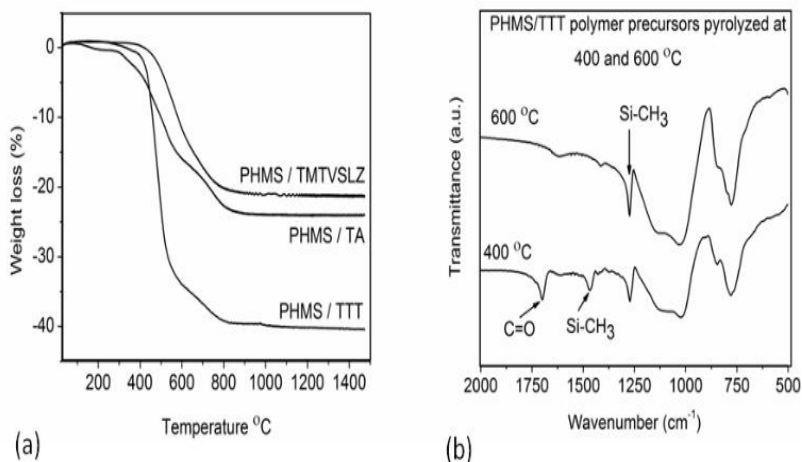
Figure 23: (a) TGA of the three pre-ceramic polymer precursors in nitrogen, and (b) FT-IR of the PHMS/TTT precursor pyrolyzed at 400 and 600 °C.

The TG curves shown in Figure 23a clearly indicate that ceramic yield depends on the structure of the pre-ceramic polymer precursors. The PHMS/TMTVSLZ gel exhibits not only the highest ceramic yield (79 %) but also the highest onset degradation temperature (400 °C). It can be due to high thermal stability of the Si-C, Si-O and Si-N bonds in the cross-linked polymer. The PHMS/TA gel shows a slightly less ceramic yield (76 %), and the weight loss process starts at about 120 °C, at which the evaporation of some low molecular weight molecules can take place. The PHMS/TTT gel shows the lowest ceramic yield (60 %) but the onset temperature for the degradation process is found to be at about 280 °C. The major difference in the mass loss pathway of these polymer precursors occurs between 400

51

and 600 °C. In detail, about 12 % of mass loss was recorded for the first two precursors, PHMS/TMTVSLZ and PHMS/TA, from 400 to 600 °C. In contrast, a significant mass loss of 32% was observed for the PHMS/TTT precursor in this temperature range. A possible explanation for this high mass loss could be the elimination of the heavy CO groups from the TTT precursor. This hypothesis is supported by the FT-IR analysis shown in Figure 23b where C=O peak was vanished by increasing temperature from 400 to 600 °C while the Si-CH$_3$ moieties belonging to the siloxane chain are still present up to 600 °C. Two new PHMS/TTT precursors were synthesized with a ratio between Si-H and C=C of 1:1 and 1:2. It means that the amount of C=O groups in the synthesized precursors consequently increases. The TGA results of the three PHMS/TTT precursors containing different amount of C=O are shown in Figure 24. The results clearly indicate that an increase in C=O amount results in a decrease in ceramic yield, from 60% to 38 % for the precursor with ratio of Si-H/C=O = 1:1, 1:2, respectively. Moreover, the main weight loss occurs at the temperature between 400 and 600 °C. These findings suggests that the evolution of the C=O strongly influence on the ceramic yield of the PHMS/TTT precursor.
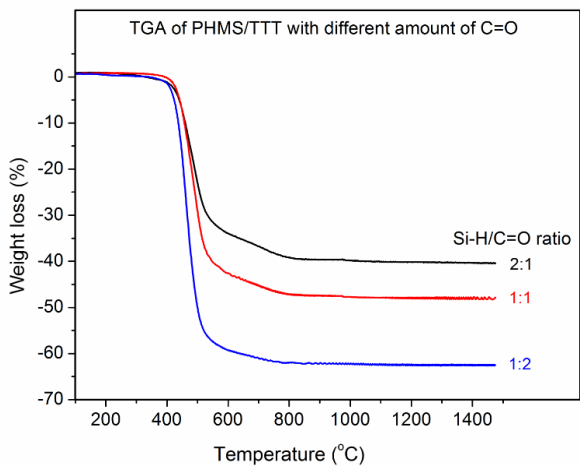
Figure 24: TGA of the PHMS/TTT polymer precursors synthesized from PHMS and TTT with different molar ratios between Si-H and C=C. The molar ratio between C=O and C=C in the TTT is equal to 1.

3.3.2 Characterization of the SiOCN ceramics

3.3.2.1 Elemental analysis

Table 3: Elemental analysis of the SiOCN samples pyrolyzed at 800 °C.

Sample	O (wt %)	C (wt %)	N (wt %)	Si (wt %)	N/Si (atomic ratio)	N/Si[†] (atomic ratio)	O/Si (atomic ratio)	O/Si[†] (atomic ratio)
PHMS/TMTVSLZ_800	20.8	21.7	4.8	52.7	0.18	0.33	0.69	0.63
PHMS/TA_800	30.4	16.9	0.5	52.2	0.02	0.11	1.02	0.63
PHMS/TTT_800	33.3	21.2	3.0	42.5	0.14	0.48	1.37	1.43

† N/Si atomic ratio in the starting precursor as obtained from the nominal chemical formula reported in Table 1.
† O/Si atomic ratio in the starting precursor as obtained from the nominal chemical formula reported in Table 1.

Chemical analysis of O, C, and N has been performed on the samples pyrolyzed at 800 °C. The results are reported in Table 3. Assuming that the H is a minor component and therefore its content can be safely disregarded, then the Si content is calculated as a difference to 100 wt%. The comparison of the experimental N/Si atomic ratio values measured for the ceramic samples with the corresponding values of the starting precursors can be taken as an indication of the ability of the polymer precursor to retain N during pyrolysis. Accordingly, in the case of the PHMS/TMTVSLZ-derived sample, N is retained in large amount, ~ 54%, compared to the calculated content in the initial precursor. The reason could be due to the stability of Si-N bonds in the precursor. On the other hand, the SiOCN sample derived from the PHMS/TA contains very low N, ~ 18%, with respect to the initial amount calculated for the precursor. The low thermal stability of N-Csp^3 bonds in the TA can be a reason for the

release of nitrogen. Another possible explanation for the low residual content of N in the PHMS/TA –derived ceramic is related to the oxygen content in the precursor. Essentially, N and O atoms are bonded to Si atoms in the ceramic structure. The number of Si atoms in the ceramics is the same as in the precursors because the loss of Si during pyrolysis can be safely neglected. Therefore, an increase in the O content in the ceramic, shown in Table 3, would induce a decrease in the residual amount of N. Interestingly, the PMHS/TTT-derived sample still retains ~ 30% of N content compared to its precursor. The stability of the bonding between N and two Csp^2 in the precursor could be a possible explanation for the better capability of retaining nitrogen in the pyrolyzed sample compared to the PHMS/TA precursor.[88]

3.3.2.2 XRD
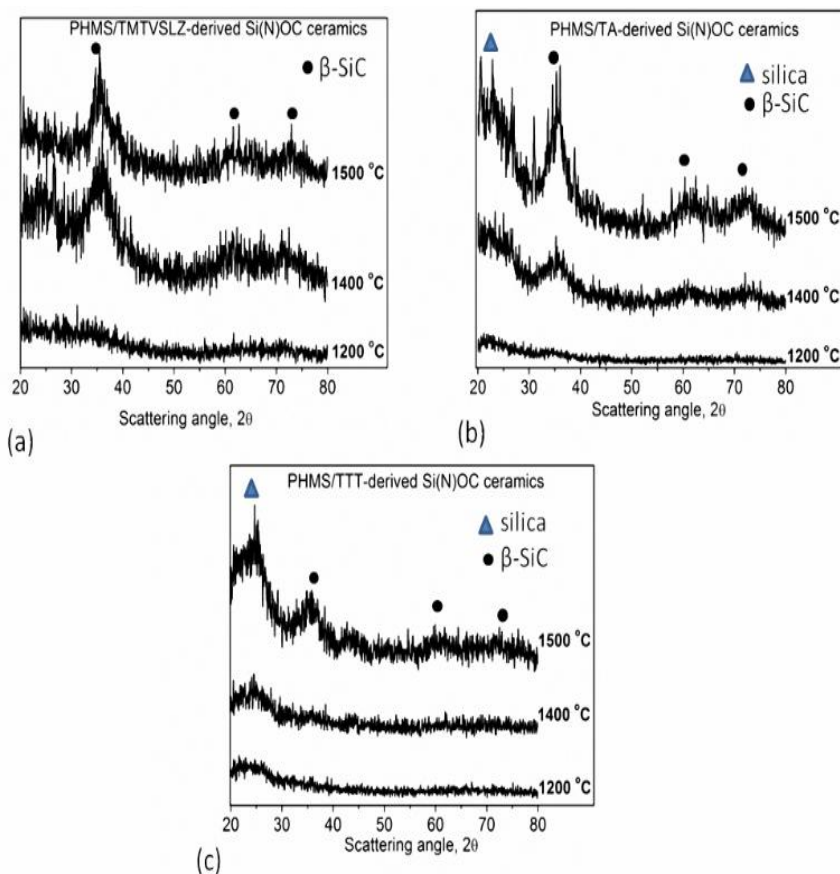
Figure 25: XRD patterns of the SiOCN ceramics derived from (a) PHMS/TMTVSLZ, (b) PHMS/TA, and (c) PHMS/TTT.

Crystallization tendency of the studied ceramics was investigated by XRD analysis. The XRD patterns of SiOCN ceramics pyrolyzed at 1200, 1400 and 1500 °C are shown in Figure 25. All the ceramic samples pyrolyzed at 1200 °C are X-ray amorphous. At 1400 °C, the PHMS/TTT -derived

ceramic is still X-ray amorphous while the PHMS/TMTVSLZ and PHMS/TA-derived samples show broad diffraction peaks indicating the onset of the crystallization process. At 1500 °C, all the ceramic samples show crystallinity evidenced by broad diffraction peaks at 2θ = 35.7; 60.4 and 72.6 °. These peaks are characteristic of nanocrystalline β-SiC. According to Scherrer equation, the average crystallite size for β-SiC is calculated to be in the range of 3 - 5 nm.

The X-ray diffraction study shows the following differences among the three samples: (i) for the PHMS/TA and PHMS/TTT compositions, a broad halo at 2θ = 22° which is clearly visible in the diffraction patterns which is assigned to the amorphous silica-based network; (ii) at 1500 °C, the intensity of the diffraction peaks of the PHMS/TMTVSLZ and PHMS/TA-derived ceramics are higher than that of the ceramic derived from PHMS/TTT. This last experimental result indicates that the TTT-derived SiOCN amorphous ceramic is more resistant toward β-SiC crystallization than the other two systems; (iii) the crystallization of Si_3N_4, is not observed for the studied ceramics.

3.3.2.3 FT-IR and ²⁹Si-NMR
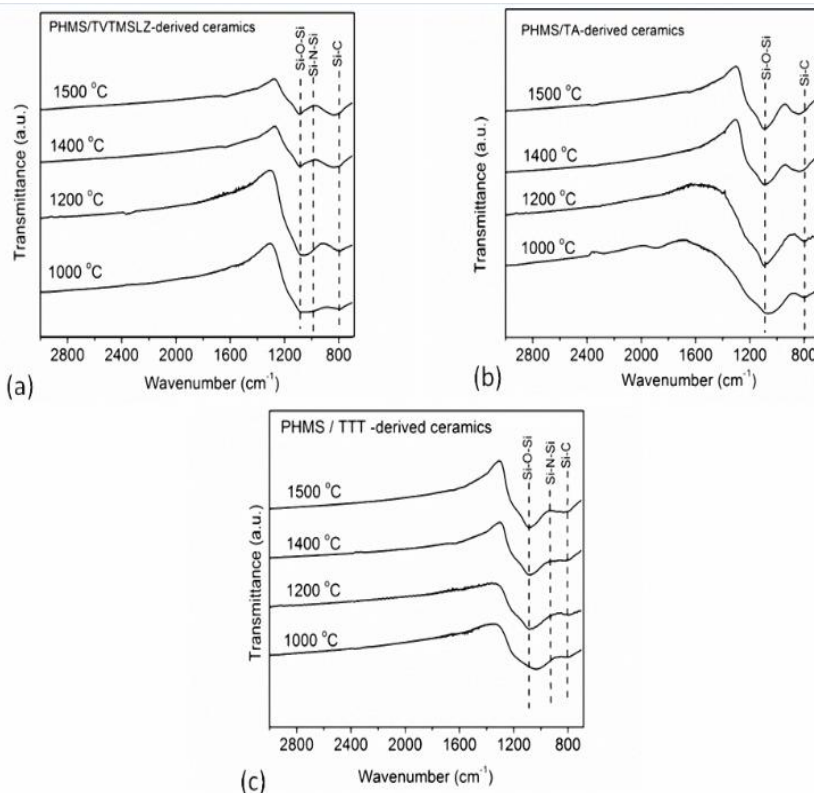
Figure 26: FT-IR spectra of the ceramics pyrolyzed at 1000, 1200, 1400 and 1500 °C: (a) PHMS / TMTVSLZ, (b) PHMS/TA, and (c) PHMS/TTT.

In order to better understand the phase separation and the SiC crystallization occurring within the ceramics at high temperature, FT-IR spectra of all the studied ceramics pyrolyzed at 1000, 1200, 1400 and 1500 °C were recorded and are shown in Figure 26. The spectrum of the PHMS/TMTVLZ pyrolyzed at 1000 °C (Figure 26a) shows very broad peaks

which could be assigned to the coexistence of Si-O, Si-N and Si-C bonds.[72] At 1200 °C, the peaks due to Si-O and Si-C bonds become more distinct while the intensity of the Si-N absorption peak at ca 920 cm^{-1} decreases suggesting that a phase separation process of the amorphous ceramic network starts at this temperature. From 1200 up to 1500 °C, the FT-IR spectra do not show any significant modification of the ceramic structure.

The FT-IR spectra (Figure 26b) of the PHMS/TA derived ceramics show, similarly to the TMTVLZ-derived samples, two main components due to Si-O and Si-C bonds. The main difference of this system with the other two is the absence of the Si-N related absorption around 920 cm^{-1}. This finding is in good agreement with the chemical analysis, which indicates that N is present in a very low amount (0.5 wt%) for this composition.

The FT-IR spectra of the PHMS/TTT-derived ceramics in Fig 26c show that increasing pyrolysis temperature does not result in a remarkable structural modification. The absorption band due to Si-C peaks appears as a very small and broad peak in all the spectra. It is due to the fact that the PHMS/TTT-derived ceramics remain amorphous structure up to 1400 °C and show low crystallinity of SiC even at 1500 °C.
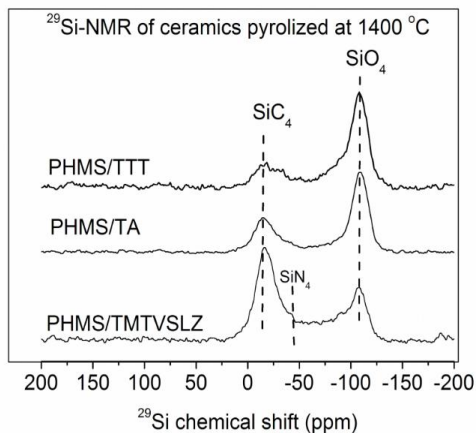
Figure 27: ^{29}Si-NMR spectra of the ceramic samples pyrolyzed at 1400 °C.

The XRD patterns indicate that the major difference in the structure among the studied ceramics occurs at the pyrolysis temperature of 1400 °C. To have more supportive information for this observation, ^{29}Si-NMR characterization was performed for all the ceramics obtained at 1400 °C (Figure 27). The NMR spectra show for all the three systems the presence of two main peaks at ca -15 and -108 ppm, which are assigned to SiC_4 and SiO_4 units, respectively. This result shows that the phase separation of the amorphous SiOCN network into SiC-rich and SiO_2-rich domains has already taken place at this temperature in all the three studied systems. The PHMS/TMTVSLZ-derived ceramic shows a quite defined peaks at δ = -16.9 ppm (SiC_4) and at -108.4 ppm (SiO_4). SiN_4 units, which should give rise to a component at -48 ppm cannot be clearly seen. For the TA- and TTT-derived SiOCN systems, the silica peak at -108.4 ppm is also well defined. On the other hand, the SiC_4 resonance becomes less intense and broadens for the TA- and TTT- derived systems. Indeed, the intensity ratio between SiC_4 and SiO_4 peaks is higher than 1 for the PHMS/TMTVSLZ and drops below 1 for the other two samples. This result is in good agreement with the XRD and

60

the FT-IR analyses. Particularly, the contribution of the SiO_4 units in the ceramic sample derived from the PHMS/TTT precursor is dominant. This is expected because the PHMS/TTT-derived ceramic remains amorphous at 1400 °C and the silicon carbide crystallization is not yet complete. Repeatedly, the ^{29}Si-NMR spectra show a coincidence with the XRD data.

3.3.2.4 XPS
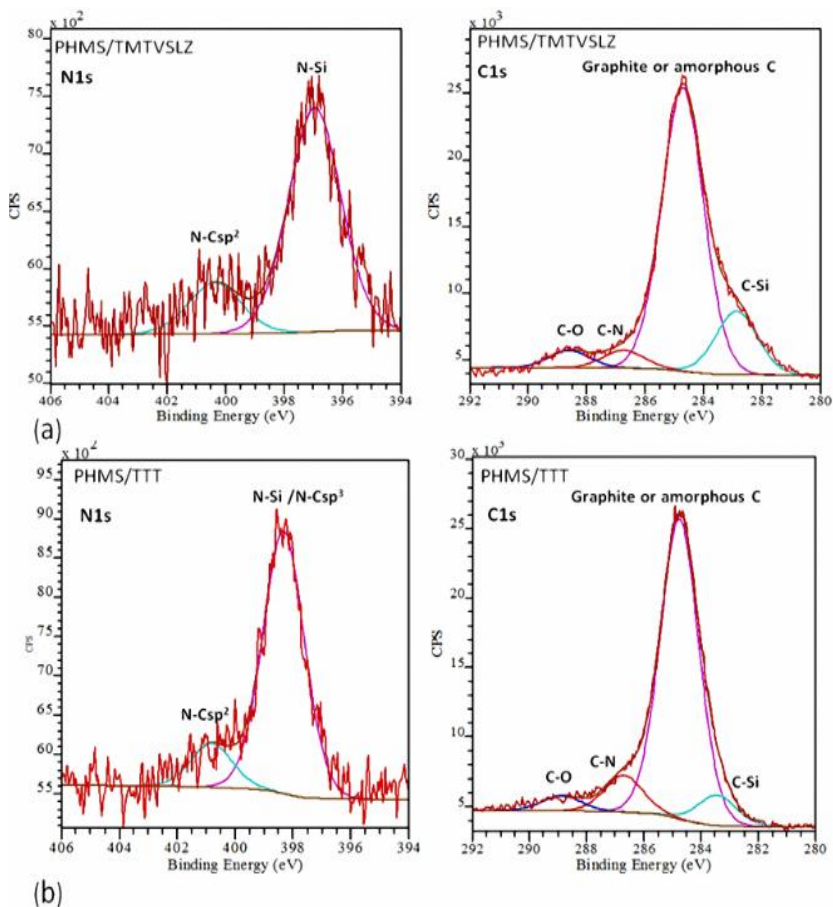
Figure 28: N1s and C1s XPS spectra of the ceramics pyrolyzed at 1000 °C from (a) PHMS/TMTVSLZ, and (b) PHMS/TTT.

To understand the chemical nature, in particular the chemical environment surrounding N atoms, XPS measurements were carried out for the two ceramic samples displaying the maximum N content, namely PHMS/TMTVSLZ and PHMS/TTT. The N1s and C1s XPS spectra recorded on the studied samples are shown in Figure 28.

For the N1s core level in the XPS spectrum of the PHMS/TMTVSLZ system, on the left side of Figure 28a, the dominant peak at 397 eV is due to N-Si bonds.[89] Interestingly, besides the major peak the N1s XPS spectrum shows another shoulder at higher binding energy (400.5 eV) which can be assigned to N-Csp^2 bonds. [89,90] It means that N atoms are mainly bonded to silicon atoms but also a smaller amount of nitrogen atoms form bonds with sp^2 carbon atoms of the free carbon phase. Whether these N-C bonds are part of the sp^2 carbon planes of the free carbon phase or form the interface between the free C and the amorphous SiOCN network is however, at present, not clear.

The C1s XPS spectrum of the same PHMS/TMTVSLZ sample, on the right side of Figure 28a, shows different chemical bonds for the C atoms with a broad range of binding energy between 282 to 290 eV. The main peak at 284.7 eV is assigned to C-C bonds in graphite or amorphous carbon.[89,91] The presence of the free carbon phase in these two studied samples was previously reported by the means of Raman and elemental analysis which are shown in the next chapter of this thesis. In the same spectrum, two shoulders are also present: at 283.5 eV, due to C-Si bonds and at 286.7 eV, due to Csp^2-N bonds, in agreement with the information obtained from the N1s XPS spectrum of the same sample. The peak at 289.1 eV is tentatively attributed to CO type bonds.[89,91]

The N1s XPS spectrum recorded for the sample derived from PHMS/TTT, on the left side of Figure 28b, reveals two different chemical bonds of N atoms. The main peak at 398.3 eV can be assigned to N-Csp^3

bonds or mixed N-Csp^3/N-Csp^2 in pyridine-like structure.[89,90] In addition, the minor peak at higher binding energy (400.8 eV) which is previously assigned to N-Csp^2 bonds also presents in the N1s XPS spectrum. However, it seems unrealistic to have only N-C bonds at such a high temperature (1000 °C). We propose that the higher binding energy of N atoms observed in this case in the N1s XPS spectrum compared to the PHMS/TMTVSLZ sample could be due to an increased proportion of N-C bonds which exist together with the N-Si bonds.[54] Since the starting precursor does not contain N-Si bonds, they must have formed during the polymer-to-ceramic transformation. It is also worth noticing that N atoms exist in different chemical bonding environments in the two precursors, i.e. as H*N*Si$_2$ in the PHMS/TMTVSLZ- and (Csp^3)*N*(Csp^2)$_2$ bonds in the PHMS/TTT. This difference seems to be maintained in the final ceramics: indeed, the SiOCN obtained from the PHMS/TTT precursor shows more N-C bonds compared to the PHMS/TMTVSLZ one. The C1s XPS spectrum recorded for the same sample, on the right side of Figure 28b, shows the formation of similar chemical bonds of C atoms as in the PHMS/TVTMSLZ sample. The presence of N in the SiOC matrix would impact on several functional properties such as electrical and optical properties. For example, the electrical conductivity of the PHMS/TTT-derived ceramics having a higher fraction of N-C bonds is higher than the values obtained for the samples derived from PHMS/TMTVSLZ at the same pyrolysis temperature.

3.4 Conclusions

SiOCN ceramics were successfully synthesized via polymer pyrolysis starting from different nitrogen-containing pre-ceramic polymers. It was found that the structure of the polymer precursors influences the thermal stability, with respect to thermal degradation, crystallization tendency of the ceramics and structural rearrangement at high temperature. Interestingly, we found that the nitrogen content and the chemical nature of the N atoms in the SiOCN ceramic samples can be controlled by the architecture of the as-synthesized precursors. In particular, we found that:

1)   the ability to retain N after pyrolysis depends on the type of bonds that N forms in the polymer precursor and follows the sequence N-Si > N-Csp^2 > N-Csp^3;

2)   Irrespectively from the type of polymer precursor, N-C bonds are present in the final ceramics, however, if in the pre-ceramic polymer N is bonded to silicon the Si-N bonds are retained to a large extent in the pyrolysis product while if N, in the pre-ceramic polymer, bonds with sp^2 carbon atoms forming N-Csp^2 bonds then a higher amount of N-C bonds are present in the SiOCN ceramic material.

Chapter 4 Physical properties and gas sensing behavior

4.1 Electrical property

4.1.1 Introduction

In the literature, electrical conductivity of the SiOC and SiCN ceramics is usually measured on small bulk components. However, it is not easy to process a crack-free monolithic PDC and a method to study the electrical properties based on powder samples would be much more suitable for these materials. According to Wang *et al.*[92] and Lu *et al.*[93] powders can be pressed and their bulk conductivity can be measured. A problem of this method is associated with the contact resistance between the particles, which leads to a high uncertainty in the measurements.[94] Recently, Ingram *et al.* proposed for the first time a method, named "Powder-Solution-Composite" (PSC) technique, in which the impedance spectroscopy was used to measure both the conductivity of a slurry, formed by mixing the studied ceramic powders and the electrolyte, and the conductivity of the electrolyte alone.[95] Then the electrical conductivity of the investigated ceramic powders was obtained by plotting the conductivity of the composite *vs* the electrolyte. The PSC method lowers the error in measuring electrical conductivity of the ceramic powders compared to the previously reported powder methods because grain boundary effect is negligible. This method has been used to measure the electrical conductivity of different ceramic powders such as $Ag_2V_4O_{11}$, $Ag_4V_2O_6F_2$, CeAgOS, BiCuOS and ZnO nanowires.[96-98] The results obtained using this method were comparable with the bulk conductivity of the same materials measured by conventional methods, for example four-point or two-point probe measurements.

In this work, the electrical conductivity of SiOCN ceramic powders derived from the PHMS/TMTVSLZ and PHMS/TTT is characterized by using PSC method. To the best of our knowledge, PSC method is applied here for the first time to study the electrical behavior of the ceramics in PDC field. The influence of the pyrolysis temperature as well as of the chemical composition of the SiOCN ceramics on their electrical conductivity is also presented. Unlike other works [99,100] in which the oxygen content was not controlled and came mostly from contamination of the polymer or during the processing steps, in the present study the oxygen was deliberately introduced into the systems from a polysiloxane.

4.1.2 Experimental

4.1.2.1 Synthesis of the ceramic powders

Two polymer precursors, PHMS/TMTVSLZ and PHMS/TTT, were synthesized as reported in chapter 2. The as-obtained cured precursors were pyrolyzed at temperatures between 1000 and 1400 °C. These two samples contain quite significant amount of N in the final ceramics. After pyrolysis, the samples were milled to obtain very fine powders for the electrical conductivity measurements.

4.1.2.2 Electrical conductivity measurements

Electrical conductivity was measured applying the PSC method. Impedance spectroscopy was applied on a slurry with different electrolyte conductivity prepared by mixing the SiOCN powders and an electrolyte. As electrolyte, an aqueous solution of Na_2SO_4 was chosen in order to have a non aggressive electrolyte (especially for the stainless steel electrodes). First Na_2SO_4 solutions with different concentrations (from 10^{-5} to 0.5 M)

were prepared. Subsequently, 20 µl of these solutions was mixed with the ceramic powders to form a composite slurry. Volume fraction of the powders was kept constant (0.75) for all measurements. The slurries were placed into a polyethylene tube (4.76 mm of internal diameter and 20 mm long), shown in Figure 29, and then carefully pressed by two stainless steel ending plugs whose ending surface were polished to mirror finish. Inner spacing between two electrodes was about 2 mm and represented the electrochemical cell with two electrodes geometry where the composite slurry was placed. The electrical impedance spectroscopy of the slurries was measured by connecting the two stainless steel electrodes to the potentiostat.
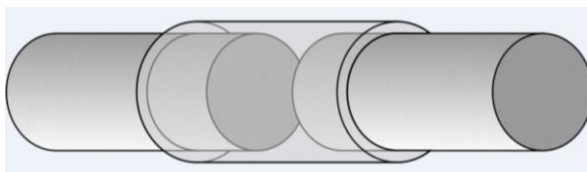
Figure 29: An apparatus for the electrical conductivity measurement.

4.1.3 Results and discussion

Table 4: Chemical compositions of the ceramic samples pyrolyzed at 1000, 1200 and 1400 °C. The uncertainty of the measurements is reported as the standard deviation. At least 5 different measurements were done for each sample.

Sample	Temp. (°C)	Si[a] (wt %)	O (wt %)	C (wt %)	N (wt %)	Empirical formula	Free C[b] (Vol %)	Amorphous SiOCN matrix (Vol%)
PHMS/TTT	1000	43.8 ± 2.3	27.8 ± 0.8	24.7 ± 1.4	3.7 ± 0.1	$SiO_{1.12}C_{1.32}N_{0.17}$	21 ± 2	79 ± 2
	1200	41.9 ± 1.0	31.5 ± 0.3	23.0 ± 0.6	3.6 ± 0.1	$SiO_{1.32}C_{1.28}N_{0.17}$	21 ± 2	79 ± 2
	1400	42.4 ± 0.6	31.5 ± 0.4	22.5 ± 0.2	3.6 ± 0.0	$SiO_{1.30}C_{1.24}N_{0.17}$	20 ± 2	80 ± 2
PHMS/TMTVSLZ	1000	51.1 ± 1.2	19.2 ± 0.5	23.6 ± 0.6	6.1 ± 0.1	$SiO_{0.66}C_{1.08}N_{0.24}$	14 ± 1	86 ± 1
	1200	51.4 ± 1.1	19.6 ± 0.4	23.0 ± 0.6	6.0 ± 0.1	$SiO_{0.67}C_{1.05}N_{0.23}$	14 ± 1	86 ± 1
	1400	49.3 ± 0.5	20.1 ± 0.3	24.0 ± 0.1	6.6 ± 0.1	$SiO_{0.72}C_{1.14}N_{0.27}$	16 ± 2	84 ± 2

[a]Uncertainty of the Si content is calculated as the sum of all the uncertainties in O, C and N contents.
[b]Free C volume is calculated based on the lower and upper limits of density values of the SiOCN amorphous matrix.

Results of the chemical analysis are reported in Table 4. There is no significant modification in chemical composition from 1000 to 1400 °C in all the investigated samples. The PHMS/TTT-derived SiOCN ceramics display a higher oxygen content and a lower nitrogen content compared to the PHMS/TMTVSLZ-derived one. The empirical formula of the ceramics is presented as $SiO_xC_yN_z$. We can express the composition $SiO_xC_yN_z$ as a mixture of $(x/2)$ mol SiO_2, $(z/4)$ mol Si_3N_4, $(1- x/2 -3z/4)$ mol SiC and $(y-1+x/2 +3z/4)$ mol C. The weight fraction of the free carbon is therefore equal to $(y-1+x/2 +3z/4)*12/(28.1 + x * 16 + y * 12 + z * 14)$ and the corresponding

weight fraction of the amorphous SiOCN network can be estimated as difference to 100%. From these values the volume fraction of the two constituents is obtained assuming a density of 2 g/cm^3 for the free-carbon phase and 2.5 g/cm^3 for the amorphous SiOCN network[1] (Note that the typical density values for the SiOCN ceramics are in the range 2 - 2.5 g/cm^3). [1] Assuming a value of 2.0 g/cm^3 for the SiOCN network the vol% of the free-carbon phase decreases to ~ 19% and ~ 13% for the PHMS/TTT and PHMS/TMTVSLZ systems, respectively).
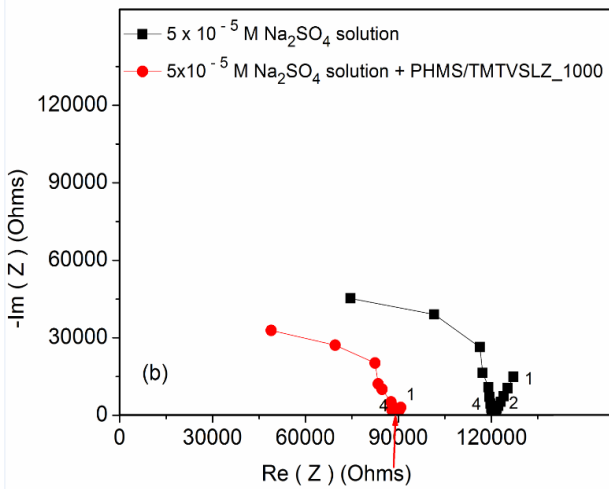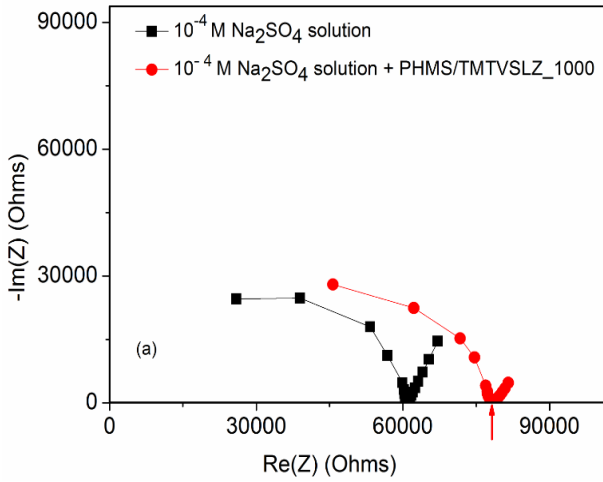
Figure 30: Experimental Nyquist plots for (a) 10^{-4} M Na_2SO_4 plain solution (squares) and 10^{-4}M Na_2SO_4 + PHMS/TMTVSLZ_1000 composite (circles), (b) $5x10^{-5}$ M Na_2SO_4 plain solution (squares) and $5x10^{-5}$ M Na_2SO_4 + PHMS/TMTVSLZ_1000 composite (circles). The composite resistance used for analysis is indicated with an arrow.

Figure 30a shows the Nyquist plots (imaginary impedance vs. real impedance) for the 10^{-4} M Na_2SO_4 plain solution and the composite formed by mixing the plain solution with 0.75 volume fraction of the ceramic powders, obtained through pyrolysis of the PHMS/TMTVSLZ precursor polymer at 1000 °C (PHMS/TMTVSLZ_1000). Frequency markers, representing log_{10} of frequency, are included in the Nyquist plots. As seen from Figure 30a, the Nyquist plot of the plain solution is formed by two components including the electrodes and the solution. The value of plain solution resistance can be obtained by using an equivalent circuit of $(R_sC_s)(R_eC_e)$, where s corresponds to the solution and e corresponds to the electrodes or taking the intersection of the spectra with the real axis, which is comparable with the four-point DC resistance of the solution.[97] The electrodes correspond to a large arc extending to low frequency (on the right, above 61106 Ω) and the solution corresponds to an arc at high frequency (on the left, below 61106 Ω). Figure 30a shows that the arc shifts to higher resistance values when the composite slurry is placed in the electrochemical cell instead of the plain solution. Since the powders are less conductive compared to the solution the composite shows a higher resistance. The cusp resistance, indicated with an arrow in Figure 30a, is considered as the composite resistance.[95,96]

Figure 30b shows the Nyquist plots for the 10^{-5} M Na_2SO_4 plain solution and the corresponding composite, (10^{-5} M Na_2SO_4+ 75 Vol% PHMS/TMTVSLZ_1000). In this case, the cusp resistance of the composite is lower than the solution's one. It means that the powders are more conductive than the solution. Therefore, we can conclude that the electrical conductivity of the PHMS/TMTVSLZ_1000 powders is between the conductivity of the plain solutions with concentration of 10^{-4} and 10^{-5} M.

It should be mentioned here that the size, size distribution and shape of the powders influence their contribution to the overall conductivity behavior of the system.[95-97] Therefore, in order to evaluate the conductivity of the studied powders, it is important to choose the appropriate model for analyzing the relation between the powders, the electrolyte and the composite. The SEM observations allow to exclude the possibility that the powders have a needle-like or a platelet-like morphology and show a roughly three-dimensional shape of PHMS/TMTVSLZ_1000 ceramic powders, as shown in Figure 31.
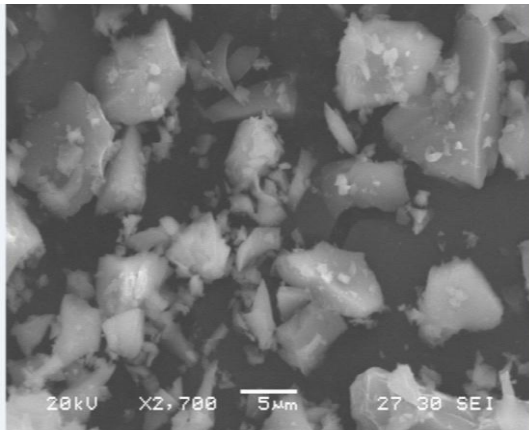
Figure 31: SEM image of the PHMS/TMTVSLZ_1000 powders.

In addition, their size varies in a broad range from hundreds of nm to a few tenths of μm. Therefore, the Bruggeman equation is chosen to model the conductivity of the system.[101]

$$\frac{K_c - K_p}{K_c^{1/3}\,(1 - K_p)} = 1 - f \quad (1)$$

Where K_c is the conductivity ratio between the slurry and the plain solution (σ_c/σ_s), K_p is the conductivity ratio between the particles and the solution (σ_p/σ_s), and f is the volume fraction of the ceramic powder which is estimated by

$$f = \frac{w/\rho}{(\pi * r^2 * l)} \quad (2)$$

Where w is the weight of the powders, ρ is the density of the powders, r is the radius of the tube used for the measurement and l is the interelectrode spacing.

The electrical conductivity of the ceramic powders can be calculated from equation (1) if the conductivity of the slurry and of the plain solution is known. However, a large error in calculation of σ_p is unavoidable because of individual error in determining both f and K_c. In order to minimize this error, a number of experiments with a wide range of the solution conductivities were carried out. This is the basis of the PSC method.
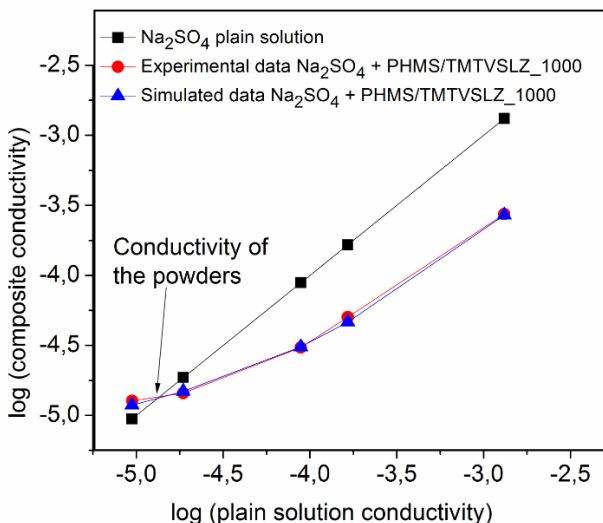
Figure 32: Experimental results of the PHMS/TMTVSLZ_ 1000 ceramic powders (circles), simulated (triangles) and plain solution (squares). The crossover point shows the powder conductivity.

Figure 32 shows that the simulated model fits well with the experimental data. The electrical conductivity of the PHMS/TMTVSLZ_1000 powders was determined to be equal to $1.35x \ 10^{-5}$ S/cm.

Experimental errors in the PSC method result from uncertainty in measuring interelectrode spacing and in reading the resistance values in the Nyquist plot. It should be mentioned that the influence of the volume fraction of the powders can be ignored if the conductivity of the powders is closed to the conductivity of the solution.[95] According to Ingram *et al.* a value of 20 % was considered as a typical error in an individual measurement. Based on this estimation, the upper and lower limits of the experimental data were calculated. To evaluate uncertainty of the experimental results, the fitting procedure using equation (1) was repeated for the upper and lower limits of the conductivity. Consequently,

conductivity of the PHMS/TMTVSLZ_1000 powder with uncertainty is $(1.35 \pm 0.15) \times 10^{-5}$ S/cm.

In order to measure the electrical conductivity of the other samples the same experimental procedures and data analyses were applied. The electrical conductivities of all the studied samples are shown in Table 5.

Table 5: Electrical conductivity of the ceramic powders, pyrolyzed from 1000 to 1400 °C.

Pyrolysis temperature (°C)	Conductivity (S/cm)	
	PHMS/TMTVSLZ	PHMS/TTT
1000	$(1.35 \pm 0.15) \times 10^{-5}$	$(4.46 \pm 0.51) \times 10^{-5}$
1100	$(7.81 \pm 0.89) \times 10^{-5}$	$(1.19 \pm 0.16) \times 10^{-4}$
1200	$(7.61 \pm 1.30) \times 10^{-4}$	$(4.57 \pm 0.68) \times 10^{-3}$
1300	$(1.39 \pm 0.34) \times 10^{-3}$	$(8.66 \pm 0.89) \times 10^{-3}$
1400	$(5.44 \pm 0.87) \times 10^{-3}$	$(1.43 \pm 0.22) \times 10^{-2}$

The studied SiOCN ceramics show conductivities in the range 10^{-5}-10^{-2} S/cm which are typical values of semiconducting materials. The electrical conductivity of each powdered ceramic sample increases by 3 orders of magnitude with increasing pyrolysis temperature from 1000 to 1400 °C. The results obtained by the PSC method, as shown in Table 6, are comparable with the values reported in literature.

Table 6: Literature values for the electrical conductivity of SiOC, SiCN, and SiOCN ceramics pyrolyzed at 1400 °C.

PDC system	Sample	Conductivity at RT (S/cm)	Measurement method	Ref.
SiOCN	Powders	$\approx 5 \times 10^{-3} - 1{,}5 \times 10^{-2}$	PSC technique	This work
SiCN	Powders	$\approx 5 \times 10^{-3}$	Microwave conductivity	[9]
SiOC	Bulk	$\approx 4 \times 10^{-3}$	Four points*	[74]
SiOCN	Bulk	$\approx 9 \times 10^{-2}$	Four points	[55]
SiCNH	Bulk	$\approx 10^{-1}$	Impedance spectroscopy	[78]
SiCN	Fragments	$\approx 10^{-1}$	Four points	[76]

In order to correlate the measured conductivity with the structure of the studied samples, Raman spectra were employed to characterize the free-carbon phase of the SiOCN ceramics (Figure 33).
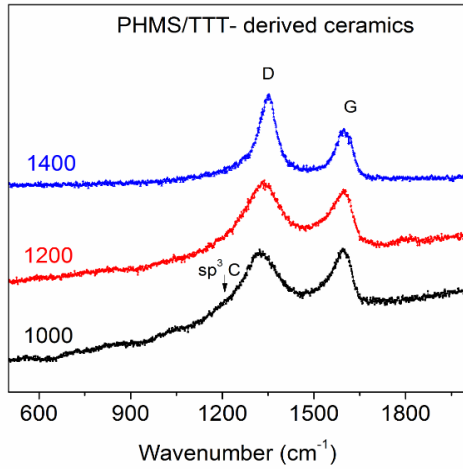
(a)
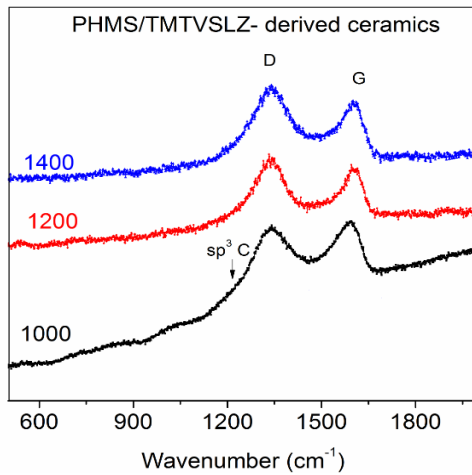
(b)

Figure 33: Raman spectra of the SiOCN ceramics pyrolyzed at 1000, 1200, and 1400 °C: (a) PHMS/TTT, and (b) PHMS/TMTVSLZ.

The Raman spectra show the appearance of the D band (1350 cm^{-1}) and the G (1600 cm^{-1}) band, which are typical for disordered graphitic-like carbon.[102] The peak intensity ratio I(D)/I(G) and full width half maximum (FWHM) of the D and G peaks are listed in Table 7.

Table 7: Variation of I(D)/I(G) ratio and FWHM line widths of the D and G peaks with pyrolysis temperature.

Sample	Pyrolysis temperature (°C)	D peak position (cm^{-1})	G peak position (cm^{-1})	I(D)/I(G)	FWHM of D peak (cm^{-1})	FWHM of G peak (cm^{-1})
PHMS/TTT	1000	1322.2	1594.3	0.99	294.5	267.9
	1200	1338.0	1596.4	1.09	255.9	175.9
	1400	1352.8	1599.6	1.59	77.7	78.8
PHMS/TMTVSLZ	1000	1335.9	1579.6	0.97	296.1	229.9
	1200	1341.2	1594.3	1.11	260.6	174.7
	1400	1352.8	1606.9	1.31	117.0	70.0

The ratio of I(D)/I(G) increases and the line widths of both the D and G bands decrease with increasing pyrolysis temperature. These observations indicate an increase in degree of ordering or in number of crystallites of the carbon phase.[56] Moreover, in the low temperature spectra (1000 and 1200 °C) the D band shows a shoulder around 1200 cm^{-1} which can be assumed as an indication of the presence of sp^{3} C atoms in the sp^{2} C structure of the graphene layers.[103,104] This shoulder can be seen up to 1200 °C but it is drastically reduced (or even totally absent) in the 1400 °C spectra suggesting that the carbon phase evolves, with the pyrolysis temperature, from an "amorphous carbon" structure toward a more "nanocrystalline graphite" structure.

In the PDC field, the electronic behavior of the ceramics is still a matter of debate: one theory suggests that the conductivity is controlled by the free-carbon phase, either forming a percolating network [56] or through a particle-matrix-particle pathway assisted by the "field concentration effect [105] while the second hypothesis points toward a key role of the amorphous silicon oxycarbonitride network.[99] Following the "free-carbon" model an enhancement of sp^3-sp^2 transformation or an increase in the ordering degree of the free-carbon phase during pyrolysis at temperatures above 1000 °C lowers the energetic barrier for the charge carrier transport leading to an increase in electrical conductivity. The activation energy for sp^3-sp^2 conversion in amorphous carbon is about 3.5 ± 0.9 eV.[106,107] A similar value, 3.3 eV, can be calculated from the conductivity of an amorphous carbon material.[104] In order to verify if the increase in conductivity with the pyrolysis temperature measured in our samples could be related to the sp^3-sp^2 conversion in the amorphous carbon phase suggested by the Raman study, we have plotted the conductivity in an Arrhenius diagram (Figure 34). The apparent activation energy is approximately 2.7 and 3.0 eV for the PHMS/TMTVSLZ and PHMS/TTT-derived SiOCN ceramics, respectively.
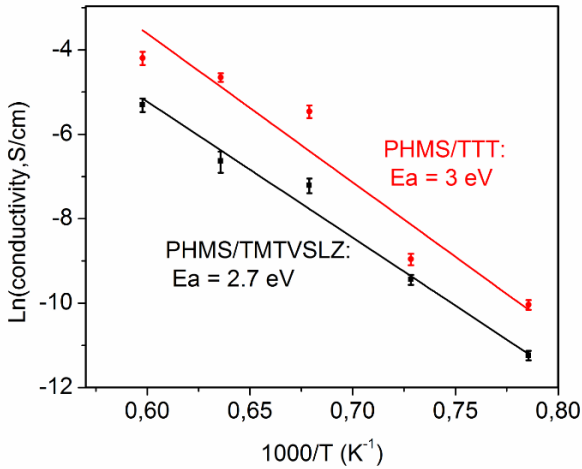
Figure 34: Arrhenius plots of electrical conductivity of the studied SiOCN ceramics.

Although these values are close to the lower limit still they support the idea that the conductivity increase is related to the sp^3-sp^2 transition of the amorphous carbon phase. A possible reason for the lower activation energy is that, contrary to most of the studies reported in the literature, the carbon structures in our samples are part of a more complex amorphous silicon oxycarbonitride network and sp^3 C atoms can share bonds with C, Si, N atoms, with residual H atoms,[54] or can just be present as sp^3 C radicals.[108] Moreover, the covalent Si-O-C-N network and the free-carbon phase can be subjected to high stresses, as it was shown for a ternary Si-B-O-C system, leading to strained bonds which could provide an extra driving force for the sp^3-sp^2 transformation.[30]

The electrical conductivity of the TTT-derived SiOCN is three to five times higher than that of the TMTVSLZ-derived ceramic at each pyrolysis temperature (Table 5).The difference in the conductivity values between the two studied systems can be discussed based on the chemical composition of the SiOCN ceramics and on the amount of the free-carbon

phase reported in Table 4. The PHMS/TMTVSLZ system has a volume percentage of free carbon slightly lower than the PHMS/TTT system. However, in both cases, the volume fraction of C_{free} is higher than the percolation threshold. Indeed, for these systems the percolating phase is constituted by graphitic-like lamellae few nm thick and the critical percolating volume is well below 10%.[56] Therefore, for both SiOCN ceramics the electronic conductivity is provided by the percolating C_{free} network. In this case, the model for the electronic conductivity of a composite material formed by a low conducting matrix and a high conductivity percolating phase indicates a little dependence of the conductivity from the vol% of the percolating phase which could be the reason why the PHMS/TTT-derived SiOCN has only a slightly higher conductivity compared to the PHMS/TMTVSLZ-derived SiOCN.[109]

Another hypothesis to explain the different conductivity of the two materials takes into account the possibility of a different conductivity of the percolating carbon-based phase. The difference between the two SiOCN systems lies in the different compounds used to introduce the nitrogen in the precursor: for the PHMS/TMTVSLZ system trimethyl-trivinyl-cyclosilazane, nitrogen is bonded to two silicon atoms and one hydrogen atom to form NSi_3 while for the PHMS/TTT composition nitrogen is introduced via triallyl-triazine-trione, in which only N-C bonds are present in CN_3 units. In the previous chapter, the XPS study showed N atoms is bonded to both Csp^2 and Csp^3 atoms in the TTT-derived ceramic sample while a small amount of N is bonded to Csp^2 in the ceramic derived from TMTVSLZ. Accordingly, a higher doping level of N into the free carbon phase presents in the TTT-derived sample compared to the TMTVSLZ-derived one. Moreover, N-doped amorphous carbon promotes the $sp^3 - sp^2$ transition which also leads to an increase in conductivity.[110] These facts are

83

reasonable explanation for a higher conductivity of the SiOCN ceramic derived from TTT compared to TMTVSLZ.

To further understand the role of the N-doped carbon phase, the PHMS/TTT precursor containing a higher content of N was synthesized from a mixture of PHMS and TTT with a Si-H/C=C ratio of 1:2, instead of 2:1 as for the precursor mentioned in the previous chapters. The N content in this as-obtained precursor (PHMS/TTT_1:2) is estimated to be 12.2 wt %. The synthesized precursor was pyrolyzed at 1000, 1200 and 1400 °C. It is expected that resulting ceramics contain a higher content of N. On the assumption that the N content in the corresponding ceramic is as half as in the precursor, as seen in the elemental analysis result for the PHMS/TTT _2:1 sample. The calculated N content in the PHMS/TTT_1:2–derived ceramics is summarized in Table 8.

Table 8: The calculated N content in the ceramics derived from the PHMS/TTT_1:2.

PHMS/TTT (Si-H/C=C)	Precursor	1000	1200	1400
2:1 (experimental data)	6.6	3.7	3.6	3.6
1:2 (calculated data)	12.1	6.8	6.8	6.8

The electrical conductivity was measured for the obtained ceramic powders. At each pyrolysis temperature, the conductivity of the PHMS/TTT_1:2-derived SiOCN ceramic is higher than that obtained for the one derived from the PHMS/TTT_2:1. The values of the electrical conductivity are shown in Table 9.

Table 9: Electrical conductivity of the ceramics derived from the PHMS/TTT_1:2. The values obtained for the PHMS/TTT_2:1-derived samples are also listed.

Pyrolysis temperature (°C)	PHMS/TTT (Si-H/C=C is 2:1)	PHMS/TTT (Si-H/C=C is 1:2)
1000	$(1.35 \pm 0.15) \times 10^{-5}$	3.63×10^{-2}
1200	$(7.61 \pm 1.30) \times 10^{-4}$	6.30×10^{-2}
1400	$(5.44 \pm 0.87) \times 10^{-3}$	1.82×10^{-1}

One possible explanation for the higher electrical conductivity of the PHMS/TTT_1:2 –derived ceramics is because of their higher carbon content. However, this reason is unlikely because the carbon content in both ceramics derived from the PHMS/TTT_1:2 or PHMS/TTT_2:1 is higher than the threshold concentration. The higher conductivity of the ceramic samples derived from the PHMS/TTT_1:2 is probably related to a higher intrinsic conductivity of the percolating carbon phase which contains a higher N concentration. To understand further, elemental analysis and XPS can be employed to determine the amount of N in these ceramics, particularly in the free carbon phase.

4.1.4 Conclusions

The electrical conductivity of the SiOCN ceramic powders derived from two pre-ceramic polymer precursors was measured for the first time using the PSC technique. The conductivity values obtained in our study are comparable with those previously reported in the literature using more conventional electrical measurements. These results suggest that the PSC

technique can indeed be applied to study the electrical properties of polymer-derived ceramics, especially of those systems for which it is impossible to obtain bulk samples.

The results show that the electrical conductivity of the SiOCN ceramics increased by 3 orders of magnitude with increasing pyrolysis temperature from 1000 to 1400 °C. The apparent activation energy for this process, estimated from an Arrhenius plot of the conductivity vs the pyrolysis temperature, is 2.7 -3.0 eV, close to the activation energy reported in the literature for the sp^3-sp^2 transition of amorphous carbon. From the chemical analysis results the presence of a percolating free-carbon phase has been assumed. The Raman study suggested the presence of sp^3 C atoms in the amorphous carbon phase, particularly at the lower pyrolysis temperatures (1000 and 1200 °C). Taken all together these data suggest that the increase in conductivity with the pyrolysis temperature is due to the sp^3-sp^2 transition occurring in the percolating free-carbon phase of the SiOCN ceramics. The higher conductivity of the PHMS/TTT-derived SiOCN compared to the PHMS/TMTVSLZ-derived ceramic could be assigned either to the slightly higher amount of free carbon in the former material or to an intrinsic higher conductivity of the percolating carbon network due to partial retention of N-C bonds with the formation of a N-doped carbon phase. The importance of N-C bonds to the electrical conductivity is quite significant. The increasing of the N content in the precursor results in the corresponding ceramics with a higher conductivity.

4.2 Optical property

4.2.1 Introduction

Heat treated SiOCNs synthesized from the reaction between a siloxane and a silazane exhibit luminescence in the visible range of 500-800 nm.[81] Ferraioli *et al* found that emission intensity of these SiOCNs is sensitive to the heating temperature. On the contrary, emission wavelength is not dependent on the treatment temperature. Interestingly, Ferraioli discovered that photoluminescence energy is higher than that of absorption. Based on these findings, the authors suggested that photoluminescence in the SiOCNs is due to mixed bond SiOCN tetrahedra whereas the absorption is related to the graphene network. However, this hypothesis is still questionable because it cannot explain the fact that if the origin of luminescence is induced by only the tetrahedral bonds why the sample heated at 400 °C does not show luminescence even though a structural modification of the SiOCN network already occurred. As mentioned in Chapter 1, the dangling bonds and the crosslinking degree of the polymers are thought to be responsible for the luminescence of the similar SiCN systems. Nevertheless, it may be not relevant to correlate the emitting centers in the SiCN and SiOCN systems because the presence of O in the SiCN matrix obviously increases the complexity of the system. For example, it is possible to have oxygen-related defects in the SiOCNs that could contribute to the luminescence properties.

The aim of the present work is to study fluorescence properties of the two series, PHMS/TMTVSLZ and PHMS/TTT. In addition, the influence of the treatment temperature and the role of the precursor structure on the fluorescence are also discussed. The relation between fluorescence and structural rearrangement in the precursor during heating is studied by FTIR.

4.2.2 Experimental

Fragments of the synthesized polymer precursors, PHMS/TMTVSLZ and PHMS/TTT, were heated at 400 and 600 °C. The obtained samples and the polymer precursors were ground to obtain fine powders. Then, they were casted on a double-sided carbon tape that was used to avoid the fluorescence arisen from the substrate. The excitation and emission spectra were recorded.

4.2.3 Results and discussion
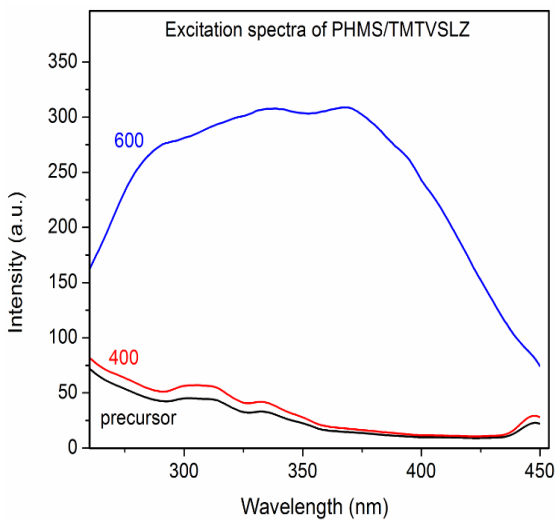
(a)
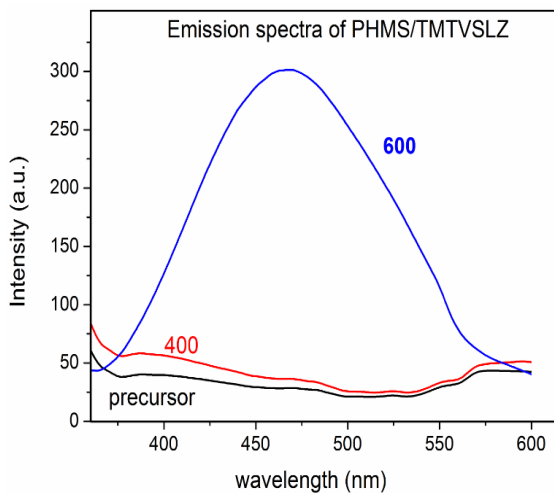
(b)

Figure 35: Fluorescence spectra of the PHMS/TMTVSLZ precursor and those heated at 400 and 600 °C: (a) excitation, and (b) emission.

The fluorescence excitation and emission spectra of the PHMS/TMTVSLZ polymer precursor and the samples heated at 400 and 600 °C are shown in Figure 35. The maximum excitation and emission wavelengths are reported in Table 10.

Table 10: Maximum excitation and emission wavelengths of the PHMS/TMTVSLZ precursor and the samples heated at 400 and 600 °C.

Sample	Excitation wavelength (nm)	Emission wavelength (nm)
PHMS/TMTVSLZ polymer	305	390
PHMS/TMTVSLZ _400 °C	305	390
PHMS/TMTVSLZ _600 °C	370	465

The PHMS/TMTVSLZ precursor and the sample heated at 400 °C (PHMS/TMTVSLZ_400) show similar excitation and emission spectra. Their excitation spectra exhibit three excitation peaks at 305 nm, 330 nm, and 450 nm. Their emission spectra are composed of two emission peaks at 390 nm, and 600 nm. As shown in Figure 35, the excitation and emission spectra of the polymer precursor and the PHMS/TMTVSLZ_400 show a very low intensity. On the contrary, the sample heated at 600 °C (PHMS/TMTVSLZ_600) shows an intense fluorescence. Its excitation spectrum presents three excitation peaks at 290 nm, 330 nm, and 370 nm. The emission spectrum of this sample shows a single broad emission peak at 465 nm. The emission spectra of the PHMS/TMTVSLZ_600 at different excitation wavelengths are shown in Figure 36. The results show similar emission spectra at different excitation wavelengths. It seems that the PHMS/TMTVSLZ_600 sample contains only type of fluorescence emitting specie that gives emission at 465 nm.
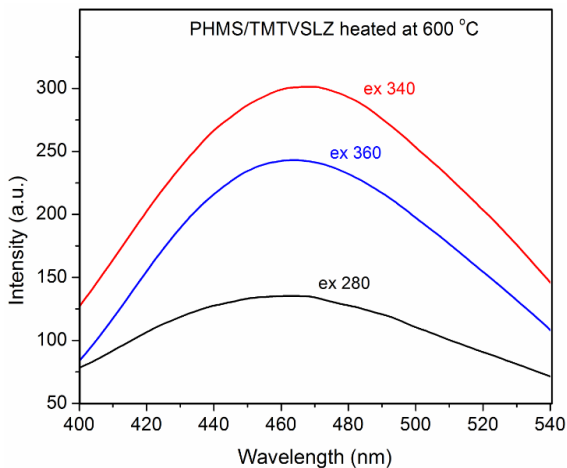
Figure 36: Emission spectra of the PHMS/TMTVSLZ_600 at different excitation wavelengths.

Obviously, the fluorescence emitting center in the PHMS/TMTVSLZ_600 sample is different from those present in the precursor and in the PHMS/TMTVSLZ_400. Since there is no emitting center present in the polymer precursor, the origin of the weak fluorescence can be caused from impurities present in the commercial products.[57] These impurities remain until up to 400 °C and lead to the same behavior of fluorescence. However, the increase of the treatment temperature to 600 °C results in a structural modification of the precursor. The structural alteration occurring between 400 and 600 °C consequently leads to the formation of new fluorescence centers. The FT-IR spectra of the polymer precursor and the heat treated samples are shown in Figure 37.
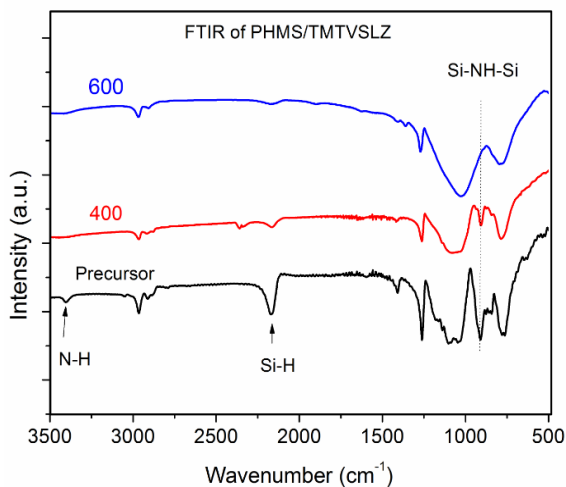
Figure 37: FT-IR spectra of the PHMS/TMTVSLZ precursor and those heated at 400 and 600 °C.

The results show that the FT-IR spectrum of the PHMS/TMTVSLZ_400 shows a reduction in intensity of the bands related to N-H, Si-H and C-H. The FT-IR spectrum of the PHMS/TMTVSLZ_600 shows the disappearance of the band corresponding to Si-NH-Si. This fact could indicate that the transamination and dehydrocoupling reactions complete between 400 and 600 °C, as shown in Scheme 9.
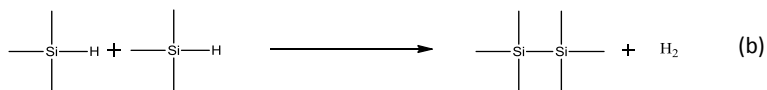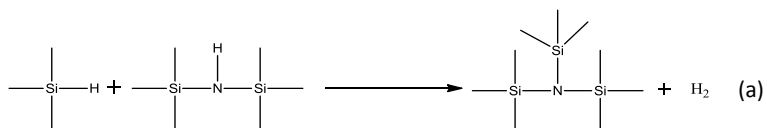
Scheme 9: (a) Transamination, and (b) dehydrocoupling reactions.

Due to the structural complexity of the SiOCN, it is a challenge to assign the origin of the fluorescence. In the literature, emitting centers are supposed to be arisen from the mixed tetrahedral bonds Si-O-C-N,[81] dangling bonds such as carbon radical,[57] oxygen-related defects,[39,111] and hydrogen-related species.[112]
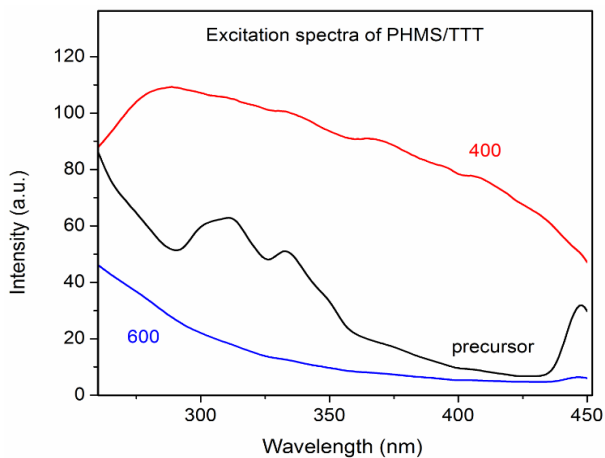
(a)
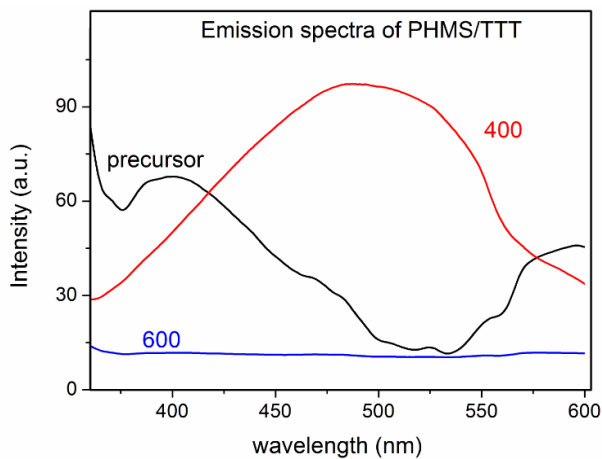
(b)

Figure 38: Fluorescence spectra of the PHMS/TTT precursor and those heated at 400 and 600 °C: (a) excitation and (b) emission.

The fluorescence excitation and emission spectra of the PHMS/TTT polymer precursor and the samples heated at 400 and 600 °C are shown in Figure 38. The maximum excitation and emission wavelengths are reported in Table 11.

Table 11: Maximum excitation and emission wavelengths of the PHMS/TTT precursor and the samples heated at 400 and 600 °C.

Sample	Excitation wavelength (nm)	Emission wavelength (nm)
PHMS/TTT polymer	310	400
PHMS/TTT_400 °C	290	490
PHMS/TTT_600 °C	-	-

The excitation spectrum of the polymer precursor exhibits three peaks at 310 nm, 333 nm, and 448 nm. The emission spectra are composed of two peaks at 400 nm and 600 nm. The sample heated at 400 °C (PHMS/TTT_400) shows a maximum excitation peak at 288 nm and other peaks at lower energies at 333 nm, 370 nm, and 407 nm. The emission spectrum of this sample is composed of a maximum emission peak at 490 nm and another possible emissions peak at 550-570 nm. The difference between the emission spectra of the PHMS/TTT polymer precursor and the PHMS/TTT_400 suggests that fluorescence emitting centers in the PHMS/TTT_400 are formed at temperatures below 400 °C. Similarly to the PHMS/TMTVSLZ, the origin of the weak fluorescence of the PHMS/TTT polymer precursor is supposed to be attributed to the impurities present in the commercial products. The assignment of the fluorescence centers present in the PHMS/TTT_400 is not easy. If the fluorescence arises from the Si-O-C network, it seem to be unlikely because there is no difference in the FT-IR spectra recorded for the precursor and the PHMS/TTT_400, as

shown in Figure 40. A similarity in the shape and the range of the emission spectra between the PHMS/TTT_400 and PHMS/TMTVSLZ_600 suggest that these samples probably contain the same emitting species. There is only a slight difference in maximum emission wavelength between the PHMS/TTT_400 and PHMS/TMTVSLZ_600. The excitation energy used for recording the emission spectra is 3.6 eV. The emission energies are 2.5 and 2.6 eV, for the PHMS/TTT_400 and the PHMS/TMTVSLZ_600, respectively. Photoluminescence has been widely studied for the systems containing Si, O, and C such as C-doped silica, SiC/SiO$_2$ and SiOC.[112-115] To have an idea about the emitting centers in the two heated SiOCNs above, the emission energy is compared with the values obtained for similar systems reported in the literature. For example, the excitation and emission energy band gap of the SiO$_2$:C layer have been shown in Figure 39.[114] The authors found that the emitting centers in this system are related to carbon. These values of band gap are close to those found in our study.
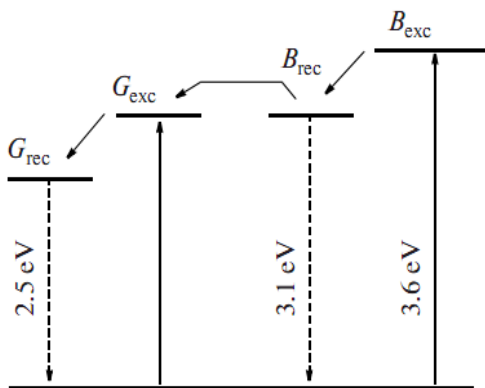
Figure 39: Schematic diagram of levels and transitions for the photoluminescence of the SiO$_2$/C layer.[114]

A slight difference in emission energy of the PHMS/TMTVSLZ_600 and the PHMS/TTT_400 could be ascribed to either the carbon concentration or the carbon-related defect levels present in these samples. The carbon content or the defect levels are shown to impact the energy band gap and therefore impact the photoluminescence of the SiOC or C-doped SiO_2 systems, as shown in Figure 39.[113,116] However, the treated samples at low temperatures contain all the Si-C, Si-O, Si-H bonds. It should not be ignored the role of the defects related to H, O, and Si. In order to characterize the type of defects present in the sample, electron paramagnetic resonance spectroscopy can be employed.

The PHMS/TTT precursor heated at 600 °C does not fluoresce due to the presence of free carbon phase which leads to the formation of black material. The presence of sp^2 carbon in this sample is verified by the FT-IR spectrum (Figure 40a) with the absorption bands at 1631 cm^{-1} and 1409 cm^{-1}. It is consistent with the Raman spectrum (Figure 40b) showing two weak peaks at 1390 cm^{-1} and 1605 cm^{-1}.
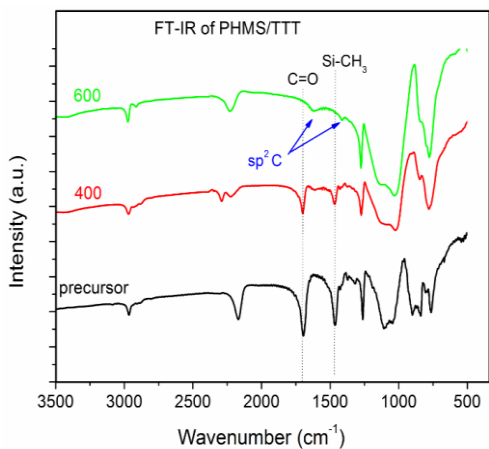
(a)
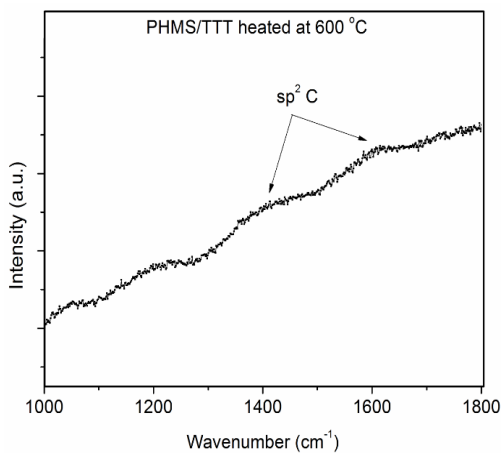
(b)

Figure 40: (a) FT-IR spectra of the PHMS/TTT precursor and those heated at 400 and 600 °C, (b) Raman spectrum of the PHMS/TTT heated at 600 °C.

4.2.4 Conclusions

The PHMS/TMTVSLZ_600 and the PHMS/TTT_400 show fluorescence in the visible range with emission peaks at 465 and 490 nm, respectively. The emitting centers in these samples are formed during the heat treatment. Depending on the structure of the precursors, the temperature to have maximum fluorescence is different. The origin of the emitting centers is supposed to be related to the carbon defects. In order to have better understanding of the emitting C-related centers, electron paramagnetic resonance spectroscopy can be employed to characterize the type of dangling bonds present in these samples.

4.3 Gas sensing behavior

4.3.1 Electrical gas sensing

The samples used for the electrical gas sensing measurements are the SiOCN ceramics obtained through pyrolysis of the PHMS/TMTVSLZ and PHMS/TTT at 1400 °C. The experimental details of the gas sensing measurement have been reported in the previous study carried out by Karakuscu *et al.*[40] The samples have been prepared using ball milling for 3h. The obtained fine powders were diluted in ethanol and consequently drop casted on an alumina substrate with the dimension of 2 mm x 2 mm x 0,25 mm. Platinum electrical contacts were placed one side of the substrate while a platinum heater was placed on the other side. *In situ* DC conductance was recorded at operating temperatures from 200 °C to 550 °C under synthetic air. The measurements were performed in a flow cell thermostated at 20 °C with a constant gas flow rate of 300 mL/min. In our study, two different target gases, NO_2 (5 ppm) and H_2 (500 ppm) have been

employed for the gas sensing test. The sensor response has been calculated as follows:

$$S = \frac{G_f - G_o}{G_o}$$

where G_0 and G_f are the steady-state conductance values measured under air and the target gas, respectively. The sample was heated at a rate of 1°C/min.
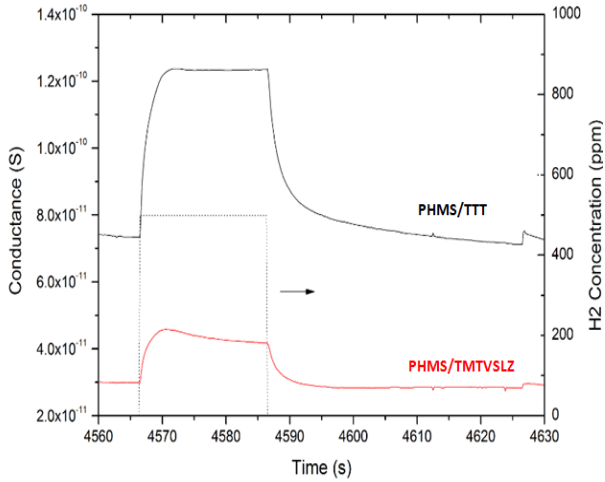
(a)
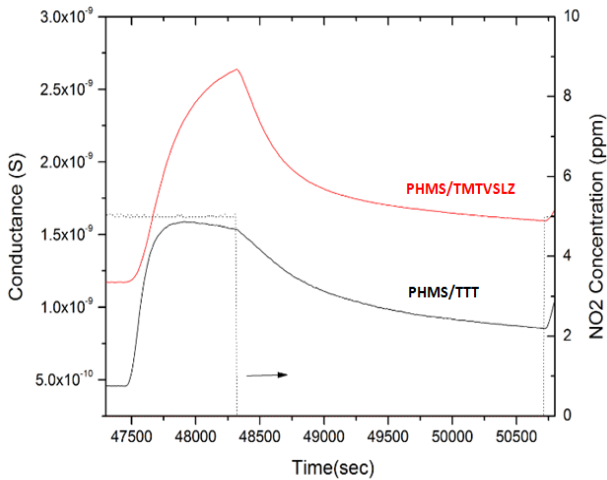
(b)

Figure 41: Dynamic response exhibited by SiOCN sensors to: (a) 500 ppm H_2 at a fixed working temperature of 450 °C, and (b) 5 ppm NO_2 at room temperature.

Figure 41 shows the gas response of the two ceramic samples toward H_2 of 5 ppm concentration and toward NO_2 of 500 ppm concentration, at the working temperature of 450 °C and room temperature, respectively. Figure 41a displays the capability of the material to detect H_2 at high temperature of 450 °C. Both of the SiOCN samples show a fast response to H_2. Conductance of the samples reaches to maximum values after 5s. The sensitivity to H_2 of the PHMS/TTT is higher than the PHMS/TMTVSLZ. Both of the samples show a reversible sensing behavior and the conductance returns to the original values with a recovery time of 5s.

Figure 41b displays the capability of the material to detect NO_2 at room temperature. Both of the SiOCN samples are sensitive to NO_2. Unlikely H_2, slower response time is observed in NO_2. Conductance of the PHMS/TTT reaches to the highest value after 50s whereas the conductance increases to only 50% of the total increase for the PHMS/TMTVSLZ in the same time. These two samples show a reversible sensing behavior to NO_2. Similarly, the sensitivity to NO_2 of the PHMS/TTT is higher than the PHMS/TMTVSLZ.
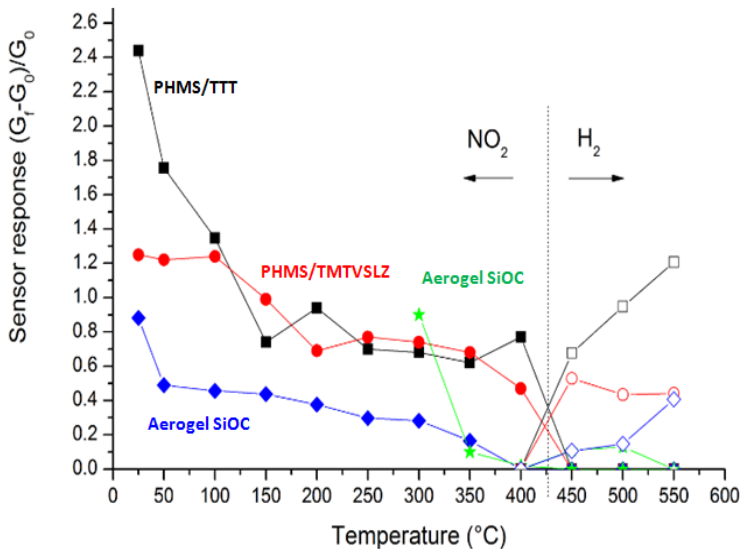
Figure 42: Gas response of the studied SiOCNs toward to NO_2 (filled dot) and H_2 (unfilled dot). The results are compared to those reported for the SiOC aerogels in the literature.

The gas response of the SiOCN to H_2 and NO_2 at different temperatures between room temperature and 550 °C is shown in Figure 42. Besides, the sensitivity of the SiOCNs is compared with that of SiOC aerogels reported in the literature. The gas response to NO_2 is the highest at room temperature and it reduces with increasing working temperature. At 450 °C, both samples are no longer sensitive to NO_2. On the contrary, the SiOCNs start to give response to the presence of H_2 at this temperature. The sensitivity to H_2 increases with increasing working temperature and reaches to the highest gas response at 550 °C. Interestingly, the studied SiOCNs are more sensitive to both NO_2 and H_2 at each measured temperature

compared to the SiOC aerogels. There are two questions arisen from these observations:

1) Why does conductance increase under the gas exposure, both of NO_2 and H_2?

2) Why does the sensitivity to NO_2 decrease with working temperature while it happens in the opposite way for H_2?

Since NO_2 is an electron-withdrawing molecule, the electron charge transfer is likely to occur from the SiOCN to NO_2. As a consequence, the hole concentration increases in the SiOCN. Taken into account the fact that conductance of the SiOCN increases upon the NO_2 exposure, SiOCN ceramics have p-type conductivity. As can be seen from Figure 42, the presence of H_2, a reducing gas, also leads to an increase in conductance of the samples. It may imply that these SiOCNs have n-type conductivity. Both p and n-type conducting behaviors are present in the SiOCNs. This result is in agreement with those reported in the previous studies in which it is believed the charge carriers in the SiOCNs can be either electrons or holes. [99] Another point can be seen from Figure 42 that conversion of p-type to n-type conductivity in the SiOCNs occurs at 450 °C. The conducting mechanism can be originated from different constituents that can be a dominant conducting phase at appropriate temperatures.

4.3.2 Optical gas sensing

The PHMS/TMTVSLZ_600 and PHMS/TTT_400 were used for the optical gas sensing study. The experimental procedures are as follows: first, the analysis chamber was purged by a flow of N_2 for 5 min. After that, emission spectrum was recorded. Then, the analysis chamber was fluxed by a flow of N_2 that was saturated with tested vapor through means of a glass bubbler filled with liquid solvent for 5 min. Subsequently, the emission spectrum in the tested vapor was recorded. In our study, two different categories of vapors including polar and non-polar organic molecules were used. All the experiments were carried out at atmospheric pressure and at room temperature. Experimental setup used for the gas sensing study is shown in Figure 43.
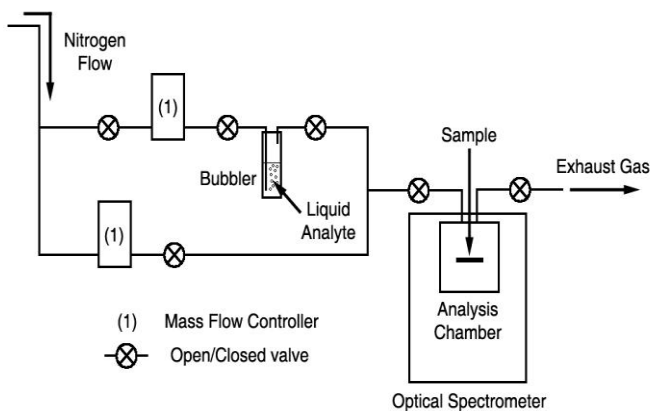
Figure 43: Experimental setup used for the gas sensing measurement (Courtesy of Prof. Alberto Quaranta, University of Trento, Italy).
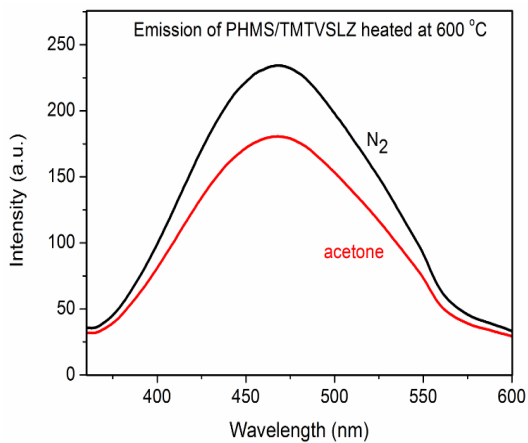
(a)
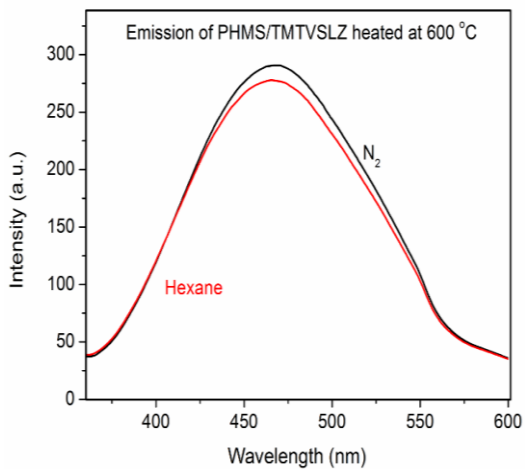
(b)

Figure 44: Emission spectra of the PHMS/TMTVSLZ_600: (a) in N_2 and in acetone saturated vapor, (b) in N_2 and in hexane saturated vapor.

Figure 44 show the fluorescence of the PHMS/TMTVSLZ_600 in N_2 atmosphere and in a mixture of N_2 and organic vapors, acetone and hexane. Adsorption of the organic vapors results in a decrease of fluorescence intensity. The quenching effect of acetone, a polar solvent, is higher than hexane, non-polar solvent. In both cases, emission wavelength does not change upon the exposure to vapors.

Fluorescence quenching mechanism in the SiOCNs is difficult to determine because of the complexity of their structure. Several processes such as energy transfer, charge transfer, molecular rearrangements, ground-state complex formation and so forth can be responsible for the quenching effect. However, the studied solvents including acetone and hexane have no accessible energy that must be necessary for the electron or charge transfer. It is unlikely that there are reactions between hexane or acetone with the heated SiOCNs. Therefore, formation of a complex between solvent and samples can be excluded. Taken into account the fact that emission wavelength remains unchanged, the quenching could be related to dipole moment of the solvent [117,118] or nonradiative traps caused by strain that is induced from the adsorption of organic solvents at the surface.[119,120] Although many studies have been published to clarify the photoluminescence quenching by the organic solvent, the mechanism is still a debate.

Similar measurements have been performed for the PHMS/TTT_400 sample. The results are shown in Figure 45. In this case, the presence of acetone results in a quenching effect with a smaller efficiency compared to the PHMS/TMTVSLZ. The exposure to hexane does not cause a decrease in fluorescence intensity. Probably, the interaction between the organic molecules and the surface of the sample is weaker.
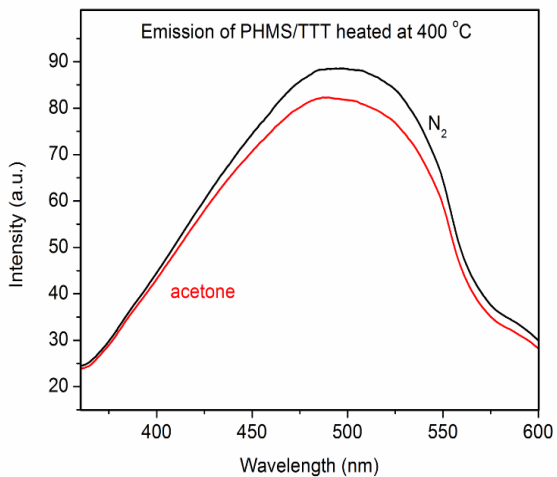
(a)
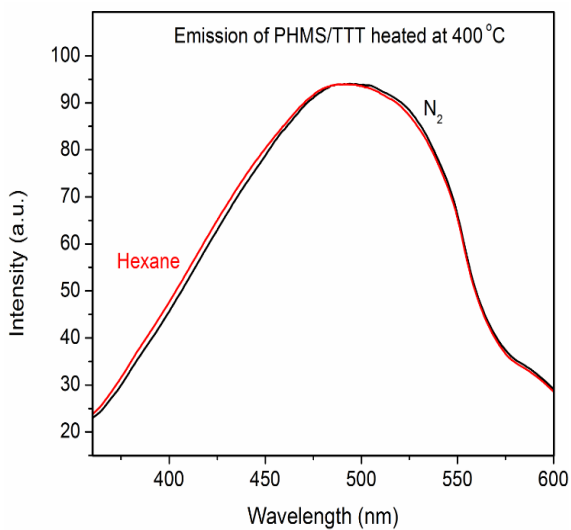
(b)

Figure 45: Emission spectra of the PHMS/TTT_400 sample: (a) in N_2 and in acetone saturated vapor, (b) in N_2 and in hexane saturated vapor.

Chapter 5 Conclusions and outlook

5.1 Conclusions

The following conclusions can be drawn from this PhD thesis:

      1.   Synthesis of the polymer preceramic precursors.

    N-doped SiOC polymer precursors were synthesized via the hydrosilylation reaction between Si-H groups in a commercial polysiloxane (PHMS) and the –CH=CH$_2$ groups in three different commercial N-containing compounds. FT-IR and NMR data confirm the successful occurrence of the synthesis.

      2.   Role of the precursor on the properties of the resulting SiOCNs

    The structure of the polymer precursors influences the thermal stability, with respect to thermal degradation, crystallization tendency of the ceramics and structural rearrangement at high temperature. The nitrogen content and the chemical nature of the N atoms in the SiOCN ceramic samples can be controlled by the architecture of the as-synthesized precursors. In particular, we found that:

    The ability to retain N after pyrolysis depends on the type of bonds that N forms in the polymer precursor and follows the sequence N-Si > N-Csp^2 > N-Csp^3;

    N atoms are bonded to Si and C atom in the final ceramics. The amount of N-C bonds is dependent on the structure of the precursors. For example, the PHMS/TMTSLZ precursor in which N is bonded to silicon, a very small amount of N-C bonds is present in the resulting ceramics.

Meanwhile, the PHMS/TTT precursor in which N is bonded to C atoms, N-Csp^2 bonds are retained in a large extent in the final ceramics.

3. Electrical and optical properties

The electrical conductivity of the SiOCN ceramics increases by 3 orders of magnitude with increasing pyrolysis temperature from 1000 to 1400 °C. The apparent activation energy for this process, estimated from an Arrhenius plot of the conductivity vs the pyrolysis temperature, is 2.7 - 3.0 eV, close to the activation energy reported in the literature for the sp^3-sp^2 transition of amorphous carbon. The increase in conductivity with the pyrolysis temperature is due to the sp^3-sp^2 transition occurring in the percolating free-carbon phase of the SiOCN ceramics.

The higher conductivity of the PHMS/TTT-derived SiOCN compared to the PHMS/TMTVSLZ-derived ceramic could be assigned either to a slightly higher amount of free carbon in the former material or to an intrinsic higher conductivity of the percolating carbon network due to partial retention of N-C bonds with the formation of a N-doped carbon phase.

The heated precursors fluoresce in the visible range with a dominant blue emission. Since the non-heated polymer precursors do not fluoresce, emitting centers must be generated during the polymer-to-ceramic transformation and they are associated with the structural changes. The origin of the luminescence could be due to C-related defects or/and Si-related defects.

4.   Gas sensing application

Regarding electrical gas sensing, the SiOCN ceramics pyrolyzed at 1400 °C are sensitive to NO_2 at temperatures below 450 °C and to H_2 at temperatures above 450 °C. The sensing behavior is reversible for both samples derived from the PHMS/TMTVSLZ and PHMS/TTT. The SiOCN ceramics show a faster response and a smaller recovery time when they were exposed to H_2 than NO_2. The SiOCNs have both n-type and p-type conductivity. The sensing mechanism is probably arisen from different components present in the ceramics, particularly the free carbon phase. In addition, the response observed for the studied SiOCN ceramics is higher than that reported in the previous studies for SiOC ceramic aerogels.

With regard to the optical gas sensing, organic vapors such as acetone and hexane can quench the fluorescence of the precursors heated at low temperatures, PHMS/TMTVSLZ_600 and PHMS/TTT_400. In conclusion, SiOCNs can be promising materials for the gas sensing application.

5.2 Outlook

The structural analysis of the SiOCN ceramic samples shows the presence of N-C bonds in the final ceramics. In order to have better characterization of the chemical structure of these ceramics, particularly the N atoms, ^{15}N-NMR should be employed. Moreover, the mechanism of remaining N in the PHMS/TTT-derived ceramic should be investigated.

The electrical conductivity of SiOCN powders at room temperature was reported. It will be interesting to have more information about conducting mechanism in these studied materials by performing the measurements at different working temperatures.

Concerning fluorescence of the samples heated at low temperatures, more investigation should be done to determine emitting centers present in these materials. For example, electron paramagnetic resonance spectroscopy could be a helpful tool for the study of defects.

For the electrical gas sensing application, the sensing mechanism is still not clear. The measurement can be performed at different concentrations of target gases, different exposure times to study the how these gases influence the conductance of the materials. In addition, *in situ* structural characterization during the gas sensing test should be performed.

References

[1]   P. Colombo, G. Mera, R. Riedel, and G.D. Sorarù, "Polymer-derived Ceramics: 40 yeas research and innovation in advanced ceramics" *J. Am. Ceram. Soc.,* 93, 1805-1837, 2010.

[2]   G.D. Sorarù and D. Suttor, "High Temperature Stability of Sol-Gel-Derived SiOC Glasses" *J. Sol-Gel Sci. Technol.,* 14, 69-74, 1999.

[3]   L. An, R. Riedel, C. Konetschny, H. -J. Kleebe, and R. Raj, "Newtonian Viscosity of Amorphous Silicon Carbonitride at High Temperature" *J. Am. Ceram. Soc.,* 81, 1349-1352, 1998.

[4]   S. Modena, G. D. Sorarù, Y. Blum, and R. Raj, "Passive Oxidation of an Effluent System: The Case of a Polymer-Derived SiOC" *J. Am. Ceram. Soc.,* 88, 339-345, 2005.

[5]   N. Suyal, T. Krajewski, and M. Mennig, "Sol-Gel Synthesis and Microstructural Characterization of Silicon Oxycarbide Glass Sheets with High Fracture Strength and High Modulus" *J. Sol-Gel Sci. Technol. ,* 13, 995-999, 1998.

[6]   V. L. Nguyen, V. Proust, C. Quievryn, S. Bernard, P. Miele, and G. D. Sorarù, "Processing, Mechanical Characterization, and Alkali Resistance of SiliconBoronOxycarbide (SiBOC) Glass Fibers" *J. Am. Ceram. Soc.,* 97, 3143-3149, 2014.

[7]   G. D. Sorarù, S. Modena, E. Guadagnino, P. Colombo, J. Egan, and C. G. Pantano, "Chemical Durability of Silicon Oxycarbide Glasses" *J.*

Am. Ceram. Soc., 85, 1529-1536, 2002.

[8] A. Karakuscu, R. Guider, L. Pavesi, and G. D. Sorarù, "White Luminescence from Sol-Gel- Derived SiOC Thin Films" *J. Am. Ceram. Soc.,* 92, 2969-2974, 2009.

[9] S. Trassl, G. Motz, E. Rossler, and G. Ziegler, "Characterisation of the Free-Carbon Phase in Precursors-Derived SiCN Ceramics" *J. Non-Cryst. Solids,* 261, 293-295, 2001.

[10] H. Fukui, H. Ohsuka, T. Hino, and K. Kanamura, "A Si-O-C Composite Anode: High Capabilityand Proposed Mechanism of Lithium StorageAssociated with MicrostructuralCharacteristics" *Appl. Mater. Interfaces,* 2, 998-1008, 2010.

[11] L. A. Liew, V.M. Bright, and R. Raj, "A novel micro glow plug fabricated from polymer-derived ceramics: in situ measurement of high-temperature properties and application to ultrahigh-temperature ignition" *Sensors Actuat. A Phys.,* 104, 246-262, 2003.

[12] L. A. Liew, R. A. Saravanan, V. M. Bright, M. L. Dunn, J. W. Daily, and R. Raj, "Processing and characterization of silicon carbon-nitride ceramics: application of electrical properties towards MEMS thermal actuators" *Sensors Actuat. A Phys.,* 103,171-181, 2003.

[13] I.-K. Sung, Christian, M. Mitchell, D.-P. Kim, and P. J. A. Kenis,"Tailored macroporous SiCN and SiC structures for high-temperature fuel reforming" *Adv. Funct. Mater.,* 15, 1336-1342, 2005.

[14] R. Kolb, C. Fasel, V. L. Kunzmann, and R. Riedel, "SiCN/C-ceramic

composite as anode material for lithium ion batteries" *J. Eur. Ceram. Soc.,* 26, 3903-3908, 2006.

[15] V.S. Pradeep, M. Graczyk-Zajac, M. Wilamowska, R. Riedel, and G. D. Sorarù, "Influence of pyrolysis atmosphere on the lithium storage properties of carbon-rich polymer derived SiOC ceramic anodes" *Solid State Ionics,* 262, 22-24, 2014.

[16] G. D. Sorarù, E. Dallapiccola, and G. D. Andrea,"Mechanical Characterization of Sol–Gel-Derived Silicon Oxycarbide Glasses" *J. Am. Ceram. Soc.,* 79, 2074-2080, 1996.

[17] T. Rouxel, G. Massouras, and G. D. Sorarù, "High Temperature Behavior of a Gel-Derived SiOC Glass: Elasticity and Viscosity" *J. Sol-Gel Sci.Technol.,* 14, 87-94, 1999.

[18] K. Kanekoa, and K.-I. Kakimoto, "HRTEM and ELNES analysis of polycarbosilane-derived Si-C-O bulk ceramics" *J. Non-Cryst. Solids,* 270, 181-190, 2000.

[19] G. D. Sorarù, F. Dalcanale, R. Campostrini, A. Gaston, Y. Blum, S. Carturan,and P. R. Aravind, "Novel Polysiloxane and Polycarbosilane Aerogels via Hydrosilylation of Preceramic Polymers" *J. Mater. Chem. ,* 22, 7676-7680, 2012.

[20] C. G. Pantano, A. K. Singh, and H. Zhang, "Silicon Oxycarbide Glasses" *J. Sol-Gel Sci. Technol.,* 14, 7-25, 1999.

[21] S. K. Young, "Sol-Gel Science for Ceramic Materials" *Material Matters,* 1, 8-13, 2006.

[22] K. Kakimoto, F. Wakai, J. Bill, and F. Aldinger, "Synthesis of Si–C–O Bulk Ceramics with Various Chemical Compositions from Polycarbosilane" *J. Am. Ceram. Soc.,* 82, 2337-2341, 1999.

[23] Y. Hasegawa, M. Iimura, and S. Yajima, "Synthesis of continuous silicon carbide fibre" *J. Mater. Sci.,* 15, 720-728, 1980.

[24] R. C. P. Cubbon, "Polymeric Precursors for Ceramic Materials" Rapra Technology Ltd, Shawbury, UK, 1994.

[25] G. D. Sorarù, G. D. Andrea, R. Campostrini, F. Babonneau, and G. Mariotto, "Structural Characterization and High-Temperature Behavior of Silicon Oxycarbide Glasses Prepared from Sol-Gel Precursors Containing Si-H Bonds" *J. Am. Ceram. Soc.,* 78, 379-387, 1995.

[26] V. Belot, R. Corriu, D. Leclercq, P. H. Mutin, and A. Vioux, "Organosilicon gels containing silicon-silicon bonds, precursors to novel silicon oxycarbide compositions" *J. Non-Cryst. Solids,* 144, 287-297, 1992.

[27] V. S. Pradeep, M. Graczyk-Zajac, M. Wilamowska, R. Riedel, and G.D. Sorarù, "Influence of pyrolysis atmosphere on the lithium storage properties of carbon-rich polymer derived SiOC ceramic anodes" *Solid State Ionics,* 262, 22-24, 2014.

[28] A. Scarmi, G.D. Sorarù, and R. Raj, "The role of carbon in unexpected visco(an)elastic behavior of amorphous silicon oxycarbide above 1273 K" *J. Non-Cryst. Solids,* 351, 2238-2243, 2005.

[29] A. Saha, R. Raj, and D. L. Williamson, "A Model for the Nanodomains in Polymer-Derived SiCO" *J. Am. Ceram. Soc.,* 89, 2188-2195, 2006.

[30] G.D. Sorarù, R. P. Alonso, and M. Leoni, "C-rich micro/mesoporous Si (B)OC: in situ diffraction analysis of the HF etching" *Micorpor. Mesopor. Mat.,* 172, 125-130, 2013.

[31] G. D. Sorarù , R. P. Alonso, and H.-J. Kleebe, "The effect of annealing at 1400 °C on the structural evolution of porous C-rich silicon (boron)oxycarbide glass," *J. Eur. Ceram. Soc.,* 32, 1751-1757, 2012.

[32] S.J. Widgeon, S. Sen, G. Mera, E. Ionescu,R. Riedel, and A. Navrotsky, "^{29}Si and ^{13}C Solid-State NMR Spectroscopic Study of Nanometer-Scale Structure and Mass Fractal Characteristics of Amorphous Polymer Derived Silicon Oxycarbide Ceramics" Chem. Mater., 22, 6221-6228, 2010.

[33] G. M. Renlund, S. Prochazka,and R. H. Doremus, "Silicon oxycarbide glasses: Part II. Structure and properties" *J. Mater. Res.,* 6, 2723-2734, 1991.

[34] J. Cordelair, and P. Greil, "Electrical conductivity measurements as a microprobe for structure transitions in polysiloxane derived Si–O–C ceramics" *J. Eur. Ceram. Soc.,* 20, 1947-1957, 2000.

[35] K. Wang, B. Ma, Y. Wang and L. An, "Complex Impedance Spectra of Polymer-Derived Silicon Oxycarbides" *J. Am. Ceram. Soc.,* 96, 1363-1365, 2013.

[36] P. Colombo, R. Riedel, G.D. Sorarù, and H.-J. Kleebe, "Polymer derived

ceramics: From nano-structure to applications" in *Optical properties*, Lancester, USA, DEStech Publications Inc, 2010, p. 253.

[37] M. Narisawa,S. Watase, K. Matsukawa, T. Dohmaru, and K. Okamura, "White Si-O-C(-H) Particles with Photoluminescence Synthesized by Decarbonization Reaction on Polymer Precursor in a Hydrogen Atmosphere" *Bull. Chem. Soc. Jpn.,* 85, 724-726, 2012.

[38] M. Narisawa, T. Kawai, S. Watase, K. Matsukawa, T. Dohmaru, K. Okamura, and A. Iwase, "Long-Lived Photoluminescence in Amorphous Si–O–C(–H) Ceramics Derived from Polysiloxanes" *J. Am. Ceram. Soc.,* 95, 3935-3940, 2012.

[39] V. Nikas, S. Gallis, M. Huang, A. E. Kaloyeros, A. P. D. Nguyen, A. Stesmans, and V. V. Afanas'ev,"The origin of white luminescence from silicon oxycarbide thin films" *Appl. Phys. Lett.,* 104, 061906, 2014.

[40] A. Karakuscu, A. Ponzoni, P. R. Aravind, G. Sberveglieri, and G. D. Sorarù, "Gas Sensing Behavior of Mesoporous SiOC Glasses" *J. Am. Ceram. Soc.,* 96, 2366-2369, 2013.

[41] C. R. Krüger, and E. G. Rochow, "Polyorganosilazanes" *J. Polym. Sci. A,* 2, 3179-3189, 1964.

[42] K. A. Andrianov, and G. V. Kotrelev, "Synthesis and properties of organocyclosilazanes" *J. Organomet. Chem.,* 7, 217-225, 1967.

[43] G. T. Burns, T. P. Angelotti, L. F. Hanneman, G. Chandra, and J. A. Moore, "Alkyl- and arylsilsesquiazanes: effect of the R group on polymer degradation and ceramic char composition" *J. Mater. Sci.,*

22, 2609-2614, 1987.

[44] R. Riedel, G. Mera, R. Hauser, and A. Klonczynski , "Silicon-based polymer-derived ceramics: Synthesis properties and applications" *J. Ceram. Soc. Jpn.,* 114, 425-444, 2006.

[45] Y. Blum , and R. M. Laine, "Catalytic methods for the synthesis of oligosilazanes" *Organometallics,* 5, 2081-2086, 1986.

[46] Y. D. Blum, K. B. Schwartz, and R. M. Laine, "Preceramic polymer pyrolysis" *J. Mater. Sci.,* 24, 1707-1718, 1989.

[47] A. O. Gabriel, R. Riedel, S. Storck ,and W. F. Maier, "Synthesis and thermally induced ceramization of a non-oxidic poly(methylsilsesquicarbodi-imide) gel" *Appl. Organomet. Chem.,* 11, 883-841, 1997.

[48] R. Riedel, A. Greiner, G. Miehe, W. Dressler, H. Fuess, J. Bill, and F. Aldinger,"The First Crystalline Solids in the Ternary Si-C-N System" *Angew. Chem. Int. Ed.,* 36, 603-606, 1997.

[49] S. Traßl, D. Suttor, G. Motz, E. Rössler , and G. Ziegler, "Structural characterisation of silicon carbonitride ceramics derived from polymeric precursors" *J. Eur. Ceram. Soc.,* 20, 215-225, 2000.

[50] J. Seitz, J. Bill, N. Egger, and F. Aldinger, "Structural investigations of Si/C/N-ceramics from polysilazane precursors by nuclear magnetic resonance" *J. Eur. Ceram. Soc.,* 16, 885-891, 1996.

[51] J. Bill, J. Seitz, G. Thurn, J. Dürr, J. Canel, B. Z. Janos, A. Jalowiecki, D.

Sauter, S. Schempp, H. P. Lamparter, J. Mayer, and F. Aldinger, "Structure Analysis and Properties of Si-C-N Ceramics Derived from Polysilazanes" *Phys. Status Solidi A.,* 166, 269-296, 1998.

[52]   Y. Iwamoto, W. Völger, E. Kroke, R. Riedel, T. Saitou and K. Matsunaga, "Crystallization Behavior of Amorphous Silicon Carbonitride Ceramics Derived from Organometallic Precursors" *J. Am. Ceram. Soc.,* 84, 2170-2178, 2001.

[53]   G. Mera, A.Tamayo, H. Nguyen, S. Sen, and R. Riedel, "Nanodomain Structure of Carbon-Rich Silicon Carbonitride Polymer-Derived Ceramics" *J. Am. Ceram. Soc.,* 93,1169-1175, 2010.

[54]   G. Mera, A. Navrotsky, S. Sen, H.-J. Kleebe and R. Riedel, "Polymer-derived SiCN and SiOC ceramics – structure and energetics at the nanoscale" *J. Mater. Chem. A,* 1, 3826-3836, 2013.

[55]   C. Haluschka, C. Engel, and R. Riedel, "Silicon carbonitride ceramics derived from polysilazanes Part II. Investigation of electrical properties" *J. Eur. Ceram. Soc.,* 20, 1365-1374, 2000.

[56]   S. Trassl, M. Puchinger, E. Rössler, and G. Ziegler, "Electrical properties of amorphous SiCxNyHz-ceramics derived from polyvinylsilazane" *J. Eur. Ceram. Soc.,* 23, 781-789, 2003.

[57]   I. Menapace, G. Mera, R. Riedel, E. Erdem, R.-A. Eichel, A. Pauletti,and G. A. Appleby, "Luminescence of heat-treated silicon-based polymers: promising materials for LED applications" *J. Mater. Sci.,* 43, 5790-5796, 2008.

[58] G. Mera, I. Menapace, S. Widgeon, S. Sen, and R. Riedel, "Photoluminescence of as-synthesized and heat-treated phenyl-containing polysilylcarbodiimides: role of crosslinking and free carbon formation in polymer-derived ceramics" *Appl. Organomet. Chem.,* 27, 630-638, 2013.

[59] V.L. Nguyen, E. Zera, A. Perolo, R. Campostrini, and G. D. Sorarù, "SiCN(O) aerogel: synthesis,characterization and gas sensing application" *J. Eur. Ceram. Soc., (Under review)*

[60] Y. Gao,H. Bai, G. Shi, "Electrosynthesis of oligo(methoxyl pyrene) for turn-on fluorescence detection of volatile aromatic compounds" *J. Mater. Chem.,* 20, 2993-2998, 2010.

[61] B. J. Birks, "Photophysics of aromatic molecules" Wiley Interscience , London, UK 1970.

[62] G. D. Sorarù, F. Babonneau, S. Maurina, and J. Vicens, "Sol-Gel synthesis of SiBOC glasses" *J. Non-Cryst. Solids,* 224,173-183, 1998.

[63] C. Gervais, F. Babonneau, N. Dallabona and G.D. Sorarù, "Sol-Gel-derived Silicon-Boron Oxycarbide Glasses Containing Mixed Silicon Oxycarbide (SiCxO4-x) and Boron Oxycarbide (BCyO3-y) Units" *J. Am. Ceram. Soc.,* 84, 2160-2164, 2001.

[64] R. P. Alonso, G. Mariotto, C. Gervais, F. Babonneau, and G. D. Sorarù, "New Insights on the high temperature nanostructure evolution of SiOC and B-doped SiBOC Polymer-derived Glasses" *Chem. Mater.,* 19, 5694-5702, 2007.

[65]   R. Riedel, A. Kienzle, W. Dresseler, L. Ruwisch, J. Bill, and F. Aldinger, "A silicoboron carbonitride ceramic stable to 2,000°C" *Nature,* 382, 796-798, 1996.

[66]   M. Weinmann , J. Schuhmacher ,H. Kummer , S. Prinz , J. Peng , H. J. Seifert , M. Christ , K. Müller , J. Bill ,and F. Aldinger , "Synthesis and Thermal Behavior of Novel Si−B−C−N Ceramic Precursors" *Chem. Mater.,* 12, 623-632, 2000.

[67]   H. J. Seifert, J. Peng, J. Golczewski, and F. Aldinger, "Phase equilibria of precursor-derived Si–(B–)C–N ceramics" *Appl. Organomet. Chem.,* 15, 794-808, 2001.

[68]   H. J. Seifert, H. L. Lukas, and F. Aldinger, "Development of Si-B-C-N ceramics supported by phase diagrams and thermochemistry" Berichte der Bunsengesellschaft für physikalische Chemie , 102,1309-1313, 1998.

[69]   A. H. Tavakoli, R. Campostrini, C. Gervais, F. Babonneau, J. Bill, G. D. Sorarù, and A. Navrotsky, "Energetics and Structure of Polymer Derived Si-(B-)O-C Glasses: Effect of the Boron Content and Pyrolysis Temperature" *J. Am. Ceram. Soc. ,* 97, 303-309, 2014.

[70]   A.H. Tavakoli, P. Gerstel1, J.A. Golczewski, and J. Bill, "Kinetic effect of boron on the thermal stability of Si–(B–)C–N polymer-derived ceramics" *Acta Materialia,* 58,6002-6011, 2010.

[71]   A. Karakuscu, R. Guider, L. Pavesi, and G. D. Sorarù, "Broad-band tunable visible emission of sol–gel derived SiBOC ceramic thin films"

Thin Solid Films, 519, 3822-3826, 2011.

[72] A. Klonczynski, G. Schneider, R. Riedel, and R. Theissmann, "Influence of Boron on the Microstructure of Polymer Derived SiCO Ceramics" *Adv. Eng. Mater.,* 6, 64-68, 2004.

[73] M. A. Schiavon, K. J. Ciuffi, and I. V. P. Yoshida, "Glasses in the Si-O-C-N system produced by pyrolysis of polycyclic silazane/siloxane networks" *J. Non-Cryst. Solids,* 353, 2280-2288, 2007.

[74] G. Wen, H. Bai, X. Huang and Z. Han, "Lotus-Type Porous SiOCN Ceramic Fabricated by Undirectional Solidification and Pyrolysis" *J. Am. Ceram. Soc.,* 94, 1309-1313, 2011.

[75] H. J. Cheng, K. Lippe, E. Kroke, J. Wagler, G. W. Fester, Y. L. Li, M. R. Schwarz, T. Saplinova, S. Herkenhoff, V. Ischenko. and J. Woltersdorf, "Sol–gel derived Si/C/O/N-materials: molecular model compounds, xerogels and porous ceramics" *Appl. Organomet. Chem.,* 25,735-747, 2011.

[76] G. Chollon, "Oxidation behaviour of ceramic fibres from the Si-C-N-O system and related sub-systems" *J. Eur. Ceram. Soc.,* 20, 1959-1974, 2000.

[77] Y. Wang, T. Jiang, L. Zhang and L. An, "Optical Absorption in Polymer-Derived Amorphous Silicon Oxycarbonitrides" *J. Am. Ceram. Soc.,* 92, 3111-3113, 2009.

[78] D. Mocaer, R. Pailler, R. Naslain, C. Richard, J. P. Pillot, J. Dunogues, O. Delverdier, and M. Monthioux, "Si-C-N ceramics with a high

microstructural stability elaborated from the pyrolysis of new polycarbosilazane precursors" *J. Mater. Sci.,* 28, 2639-2653, 1993.

[79] T. Varga, A. Navrotsky, J.L. Moats, R.M. Morcos, F. Poli, K. Mueller, A. Saha, and R. Raj, "Thermodynamically Stable SiwCxNyOz Polymer-Like, Amorphous Ceramics Made from Organic Precursors" *J. Am. Ceram. Soc.,* 90, 3213-3219, 2008.

[80] Z. L. Sun, Y. Zhou, D. C. Jia,X. M. Duan, Z. H. Yang, D. Ye, P. F. Zhang, Q. Zhang, "Mechanical and thermal physical properties of amorphous SiCN(O) ceramic bulks prepared by hot-press sintering" *Mater. Lett.,* 72, 57-59, 2012.

[81] L. Ferraioli, D. Ahn, A. Saha, L. Pavesi and R. Raj, "Intensely Photoluminescent Pseudo-Amorphous SiliconOxyCarboNitride Polymer–Ceramic Hybrids" *J. Am. Ceram. Soc.,* 91, 2422-2424, 2008.

[82] G. Socrates, "Infrared and Raman Characteristic Group Frequencies" 3rd ed., West Sussex , England : John Wiley & Sons Ltd, 2001.

[83] I. M. E. Nahhal,M. M. Chehimi, C. Cordier,and G. Dodin "XPS, NMR and FTIR structural characterization of polysiloxane-immobilized amine ligand systems" *J. Non-Cryst. Solids,* 75,142-146, 2000.

[84] P. Dibandjo, S. Diré , F. Babonneau,and G.D. Sorarù, "Influence of the polymer architecture on the high temperature behavior of SiCO glasses: A comparison between linear- and cyclic-derived precursors" *J. Non- Cryst. Solids,* 356, 132-140, 2010.

[85] N. C. K. Yive, R. J.P. Corriu, D. Leclercq, P.H. Mutin, and A. Vioux,

"Silicon Carbonitride from Polymeric Precursors: Thermal Cross-Linking and Pyrolysis of Oligosilazane Model Compounds" *J. Chem. Mater. ,* 4, 141-146, 1992.

[86]   R. Pohl, M. Dračínský, L. Slavětínská, and M. Buděšínský, "The observed and calculated 1H and 13C chemical shifts of tertiary amines and their N-oxides." *Magn. Reson. Chem.,* 49, 320-327, 2011.

[87]   T. A. Pham, D-P. Kim, T-W Lim, S-H. Park, D-Y. Yang, and K-S. Lee, " Three-Dimensional SiCN Ceramic Microstructures via Nano-Stereolithography of Inorganic Polymer Photoresists" *Adv. Funct. Mater.,* 16,1235-1241, 2006.

[88]   C. Tang, Y. Bando, D. Golberg, and F. Xu, "Structure and nitrogen incorporation of carbon nanotubes synthesized by catalytic pyrolysis of dimethylformamide" *Carbon,* 42, 2625-2633, 2004.

[89]   K. Yamamoto, Y. Koga, S. Fujiwara, "XPS studies of amorphous SiCN thin films prepared by nitrogen ion-assisted pulsed-laser deposition of SiC target" *Diamond Relat. Mater.,* 10, 1921-1926, 2001.

[90]   C. Zhang, L. Fu, N. Liu, M. Liu, Y. Wang, and Z. Liu, "Synthesis of nitrogen-doped graphene using embedded carbon and nitrogen sources" *Adv. Mater. ,* 23, 1020-1024, 2011.

[91]   G.D. Sorarù, G.D. Andrea, and A. Glisenti, "XPS characterization of gel-derived silicon oxycarbide glasses" *Mater. Lett.,* 27, 1-5, 1996.

[92]   R. Wang, A.W. Sleight, and D. Cleary, "High Conductivity in Gallium-Doped Zinc Oxide Powders" *Chem. Mater.,* 8, 433-439, 1996.

[93]   X. Lu, O. Nilsson, and J. Fricke, "Measurements of Thermal and Electrical Conductivity as well as Elastic Modulus of Electrically Conducting Powder Systems" *High Temp.-High Press.,* 23, 149-155, 1991.

[94]   J. Newmanm, "Resistance for Flow of Current to a Disk" *J. Electrochem. Soc.,* 113, 501-502, 1966.

[95]   B.J. Ingram and T. O. Mason, "Powder-Solution-Composite Technique for Measuring Electrical Conductivity of Ceramic Powders" *J. Electrochem. Soc.,* 150, 396-402, 2003.

[96]   M. I. Bertoni, N. J. Kidner, T. O. Mason, T. A. Albrecht, E. M. Sorensen, and K. R. Poeppelmeier, "Electrical and Optical Characterization of $Ag_2V_4O_{11}$ and $Ag_2V_2O_6F_2$" *J. Electroceram.,* 18, 189-195, 2007.

[97]   G. H. Chan, D. Deng, M. Bertoni, J. R. Ireland, M. C. Hersam, T. O. Mason, R. D. V. Duyne, and J. A. Ibers, "Syntheses, Structures, Physical Properties, and Theoretical Studies of CeMxOS (M= Cu, Ag; x≈ 0.8) and CeAgOS" *Inorg. Chem.,* 45, 8264-8272, 2006.

[98]   W. C. Sheets, E. S. Stampler, H. Kabbour, M. I. Bertoni, L. Cario, T. O. Mason, T. J. Marks, and K. R. Poeppelmeier, "Facile Synthesis of BiCuOS by Hydrothermal Methods" *Inorg. Chem.,* 46, 10741-10748, 2007.

[99]   H.Y. Ryu, Q. Wang, and R. Raj, "Ultrahigh-Temperature Semiconductors Made from Polymer-Derived Ceramics" *J. Am. Ceram. Soc.,* 93, 1668-1676, 2010.

[100] L. Zhang, Y. Wang, Y. Wei, W. Xu, D. Fang, L. Zhai, K.-C. Lin, and L. An, "A Silicon Carbonitride Ceramic with Anomalously High Piezoresistivity" *J. Am. Ceram. Soc.,* 91, 1346-1349, 2008.

[101] H. Fricke, "A Mathematical Treatment of the Electric Conductivity and Capacity of Disperse Systems" *Phys. Rev.,* 24, 575-587, 1924.

[102] A.C. Ferrari and J. Robertson, "Interpretation of Raman Spectra of Disordered and Amorphous Carbon" *Phys. Rev. B.,* 61, 14095-14107, 2000.

[103] A. Sadezky, H. Muckenhuber, H. Grothe, R. Niessner, and U. Poschl, "Raman Microspectroscopy of Soot and Related Carbonaceous Materials: Spectral Analysis and Structural Information" *Carbon,* 43, 1731-1742, 2005.

[104] Y. Inoue, M. Sugano, S. Kawakami, M. Kitano, K. Nakajima, H. Kato, and M. Hara, "Electrical Properties of Amorphous Carbon Semiconductor Prepared Using a Naphthalene Precursor" *"Bull. Chem. Soc. Jpn,* 86, 45-50, 2013.

[105] Y. Chen, F. Yang, and L. An, "On Electric Conduction of Amorphous Silicon Carbonitride Derived from a Polymeric Precursor" *Appl. Phys. Lett.,* 102, 231902, 2013.

[106] A. C. Ferrari, S. E. Rodil, J. Robertson, and W. I. Milne, "Is Stress Necessary to Stabilise sp3 Bonding in Diamond-like Carbon" *Diamond Relat. Mater.,* 11, 994-999, 2002.

[107] D. S. Grierson, A. V. Sumant, A. R. Konicek, T. A. Friedmann, J. P.

Sullivan, and R. W. Carpick, "Thermal Stability and Rehybridization of Carbon Bonding in Tetrahedral Amorphous Carbon" *J. Appl. Phys.,* 107, 033523, 2010.

[108] G.D. Sorarù, F. Babonneau, and J.D. Mackenzie, "Structural Evolution from Polycarbosilane to SiC Ceramics" *J. Mat. Sci.,* 25, 3886-3893, 1990.

[109] D. S. McLachlan, "Analytical Functions for the dc and ac Conductivity of Conductor-Insulator Composites" *J. Electroceram.,* 5, 93-110, 2000.

[110] J. Hu, P. Yang, and C. M. Lieber, "Nitrogen-driven sp^3 to sp^2 Transformation in Carbon Nitride Materials" *Phys. Rev. B.,* 57, 3185, 1998.

[111] S. Gallis, V. Nikas, H. Suhag, M. Huang, and A. E. Kaloyeros, "White light emission from amorphous silicon oxycarbide (a-SiCxOy) thin films: Role of composition and postdeposition annealing" *Appl. Phys. Lett.,* 97, 081905, 2010.

[112] Y. D. Glinka, S.-H. Lin, and Y.-T. Chen, "The photoluminescence from hydrogen-related species in composites of SiO_2 nanoparticles" *Appl. Phys. Lett.,* 75, 778, 1999.

[113] F. Devynck, A. Alkauskas, P. Broqvist, and A. Pasquarello, "Defect levels of carbon-related defects at the SiC/SiO_2 interface from hybrid functionals" *Phys. Rev. B,* 83, 195319, 2011.

[114] A. V. Vasin, V. I. Kushnirenko, V. S. Lysenko, A. N. Nazarov, Y. Ishikawa, and J. Salonen, "The nature of white luminescence in SiO_2:C

layers" *Tech. Phys. Lett.,* 35, 559-562, 2009.

[115] W. H. Green, K. P. Le, J. Grey, T. T. Au, and M. J. Sailor, "White Phosphors from a Silicate-Carboxylate Sol-Gel Precursor That Lack Metal Activator Ions" *Science,* 276, 1826-1828, 1997.

[116] S.-Y. Seo, K.-S. Cho, and J. H. Shin, "Intense blue–white luminescence from carbon-doped silicon-rich silicon oxide" *Appl. Phys. Lett.,* 84, 717, 2004.

[117] J. M. Lauerhaas , G. M. Credo , J. L. Heinrich , and M. J. Sailor, "Reversible luminescence quenching of porous silicon by solvents" *J. Am. Chem. Soc,* 114, 1911-1912, 1992.

[118] J.-N. Chazalviel, F. Ozanam and V. M. Dubin , "Role of dielectric effects in the red-green switching of porous silicon luminescence" *J. Phys. I France,* 4, 1325-1339, 1994.

[119] D. Bellet, and G. Dolino, "X-ray observation of porous-silicon wetting" *Phys. Rev. B,* 50, 17162, 1994.

[120] J. M. Rehm, G. L. McLendon, L. Tsybeskov, and P. M. Fauchet, "How Methanol Affects The Surface Of Blue And Red Emitting Porous Silicon" *Appl. Phys. Lett.,* 66, 3669, 1995.

Acknowledgements

In the first place, I would like to express my sincere gratitude to my supervisor, Prof. Gian Domenico Sorarù for giving me a great opportunity to work in his group. Prof. Sorarù has been continuously giving me helpful advices and supporting during my PhD. Without his great encouragement and supports, I could not finish this thesis! I also would like to acknowledge European Community ITN7 through MC-ITN FUNEA-Project 26487 for financial support. Moreover, I also would like to acknowledge to all the people who have helped me during my PhD:

Dr. Caterina Zanella from the University of Trento for her help with the impedance spectroscopy measurement.

Dr. Paolo Bettotti from the University of Trento for his help with the Raman measurement.

Dr. Nadhira Bensaada Laidani from Fondazione Bruno Kessler in Trento,Italy for her XPS measurement.

Mr. Wenjie Li from the Technical University of Darmstadt, Germany for his help in elemental analysis.

Dr Emanuela Carolline of the University of Trento for her NMR measurement.

Dr Aylin Karakuscu from the University of Brescia for her electrical gas sensing measurement.

Professor Thomas Mason from the Northwestern University, USA and Professor Marianna Bertoni from the Arizona State University, USA for their helpful suggestions.

I am thankful to all my colleagues in the ceramic laboratory: Emanuele, Pradeep, Kiran, Evgeny, John, Praneysh, Anshu, Rahul, Dawit and other researchers in the Department of Industrial Engineering for their dedication in doing experimental measurements and knowledge.

I would like to give my special thanks to my girlfriend Arianna Marzatico and her parents Anna Marzatico and Andreas Covi for always being supportive during my stay in Trento.

Finally, I am grateful to my family for their supports and encouragements during my life.

Curriculum Vitae

Education

2012 - 2015: **PhD** in Material Sciences and Engineering at the Department of Industrial Engineering, University of Trento, Trento, Italy.

Dissertation: "Synthesis and characterization of multifunctional polymer-derived SiOCN"

2009 – 2011: **MSc** in Functional Advanced Materials Engineering, 1st year at the Grenoble Institute of Technology (France) and 2nd year at the Technical University of Darmstadt (Germany)

Thesis: "Molecular approaches to novel SiHfBCN ceramic nanocomposites: synthesis and high temperature behavior".

2004 - 2008: **BSc** in Chemistry (Honors program), Hanoi University of Science, Hanoi, Viet Nam

Research Experiences

11.2011 – 11.2014: Early Stage Researcher (Marie Curie Fellow) at the Department of Industrial Engineering, University of Trento, Italy

Studied: Polymer-derived ceramics for electrical/optical gas sensors (SiOCN)

Industrial trainings: AZ Electronic Materials GmbH (Germany); MDA Advanced Ceramics (Turkey); Electrolux (Italy)

Practical courses: Stockholm (Sweden); Darmstadt and Bayreuth (Germany); Montpellier (France); Bratislava (Slovakia); Padova (Italy)

06.2013 - 07.2013: Internship at the European Institute of Membrane, University Montpellier II, France
Studied: Processing of polymer-derived ceramic fibers (SiBOC)

03.2011 - 09.2011: Graduate Research Assistant at the Department of Material Science, Technical University of Darmstadt, Germany
Studied: High temperature ceramic nanocomposites (SiHfBCN)

02.2010 - 07.2010: Internship at the Lab of Science and Engineering of Materials and Processes, Grenoble Institute of Technology, France
Studied: High temperature oxidation kinetics of of FeCoNi alloys

09.2008 - 08.2009: Graduate Research Assistant at the Department of Materials Science and Engineering, Gwangju Institute of Science and Technology, Gwangju, Korea
Studied: Synthesis of block copolymers containing pyridine moieties using living anionic polymerization.

07.2007 - 06.2008: Undergraduate Research Assistant at the Vietnamese Academy of Science and Technology, Hanoi, Viet Nam
Studied: Additives for food processing and preservation

Research Interests

Ceramics for high temperature applications, Porous ceramic materials, Polymers for LED applications,

Publications

1. Van Lam Nguyen, Caterina Zanella, Paolo Bettotti, and Gian Domenico Sorarù, "Electrical Conductivity of SiOCN by the Powder-Solution-Composite Technique" J. Am. Ceram. Soc., 97 [8] 2525-30 (2014)

2. Van Lam Nguyen, Vanessa Proust, Caroline Quievryn, Samuel Bernard, Philippe Miele, and Gian Domenico Sorarù, "Processing, Mechanical Characterization and Alkali Resistance of SiliconBoronOxycarbide (SiBOC) Glass Fibers" J. Am. Ceram. Soc.,97 [10] 3143-9 (2014)

3. Van Lam Nguyen, Emanuele Zera, Andrea Perolo, Renzo Campostrini, and Gian Domenico Sorarù, "SiCN Aerogels: Synthesis, Characterization and Gas Sensing Application" (Under Review)

4. Van Lam Nguyen, Nadhira Bensaada Laidani, Gian Domenico Sorarù, " N-Doped SiOC Ceramics from Preceramic Polymers: The Role of the N-containing Precursor" (DOI: 10.1557/jmr.2015.44)

Conferences and Workshops

1. **V. L. Nguyen**, G. D. Sorarù, "Synthesis of N-doped SiOC Ceramics from Different Precursors", (Oral presentation), 6th International Workshop on Spinel Nitride and Related Materials (Germany, September 2012)

2.V. Proust, C. Quievryn, S. Bernard, **V. L. Nguyen,** G. D. Sorarù, P. Miele, "Synthesis and Structural Characterization of SiliconBoron Oxycarbide (SiBOC) Ceramic Fibers", (Oral presentation), International Glass Fiber Symposia (Germany, October 2012)

3. G. D. Sorarù, **V. L. Nguyen**, V. Proust, C. Quievryn, S. Bernard, and P. Miele, "SiBOC ceramic fibers via pyrolysis of hybrid borosiloxane gel

fibers", (Poster), 37th International Conference & Exposition on Advanced Ceramics & Composites (USA, January 2013)

4. **V. L. Nguyen,** P. Bettotti, P. Lavesi, G. D. Sorarù, "Influence of the starting precursors on high temperature of SiOCN ceramics", (Oral presentation), 13th Conference of the European Ceramic Society (France, June 2013)

5. G. D. Sorarù, A. Quaranta, S. Dire, **V. L. Nguyen**, and M. Narisawa, "Mesoporous transparent bulk SiOC processed via hydrogen decarbonisation as optical gas sensor", (Oral presentation), 38th International Conference & Exposition on Advanced Ceramics & Composites (USA, January 2014)

6**. V. L. Nguyen,** V. Proust, C. Quievryn, S. Bernard, P. Miele, and G. D. Sorarù, "Preparation of SiBOC Glass Fibers via a Sol-Gel Route: Mechanical Characterization and Alkali Resistance Behavior", (Oral presentation), 11th Workshop Italiano Sol-Gel (Italy, June 2014)

7. **V. L. Nguyen**, C. Zanella, P. Bettotti, and G. D. Sorarù, "Electrical Conductivity of SiOCN Ceramics by the Powder-Solution-Composite Technique", (Oral presentation), 8th International Symposium on Nitrides (Germany, September 2014)

8. **V. L. Nguyen**, E. Zera, A. Perolo, R. Campostrini, and G. D. Sorarù, "SiCN Aerogels: Synthesis, Characterization and Gas Sensing Application", (Oral presentation), 8th International Symposium on Nitrides (Germany, September 2014)

9. **V. L. Nguyen,** V. Proust, C. Quievryn, S. Bernard, P. Miele, and G. D. Sorarù, "New High Modulus and Alkali Resistant Glass Fibers of the Si-B-O-C System", (Oral presentation), 12th European Society of Glass Conference (Italy, September 2014)

10. **V. L. Nguyen**, V. Proust, C. Quievryn, S. Bernard, P. Miele, and G. D. Sorarù, "Processing, Mechanical Characterization and Alkali Resistance of

SiliconBoronOxycarbide (SiBOC) Glass Fibers", (Oral presentation), 6th International Workshop on Flow and Fracture of Advanced Glasses (Germany, October 2014)

Awards

2011-2014:   Marie Curie Fellowship

2009-2011:   Erasmus Mundus Scholarship

2008-2009:   IITA fellowship (awarded by the Government of Republic of Korea)

2004 – 2008:   Vietnamese scholarship for excellent students in four consecutive years

Skills

Language: Vietnamese (mother language) English (fluent), Italian (Basic), German, Korean (attended basic course)

Computer: Good at search engines, familiar with most of popular programs and packages, able to learn new computer programs quickly

Technical: Familiar with different synthesis and characterization techniques such as: Schlenk line, glove-box, NMR, XRD, FT-IR, SEM, TG/DTA, Spectrofluorometer, Impedance Spectroscopy, Furnace, Mechanical Testing Machine

References

Prof. Gian Domenico Sorarù (PhD advisor)

Dipartimento di Ingegneria Industriale, Università di Trento

Via Mesiano 77, 38123 Trento, Italy

Tel: +39 0461 282 454

Fax: +39 0461 281 977

Email: soraru@ing.unitn.it

Prof. Dr. Dr. h. c. Ralf Riedel (Master advisor)

Fachbereich Material- und Geowissenschaften, Technische Universität Darmstadt

Jovanka-Bontschits-Strasse 2, 64287 Darmstadt, Germany

Tel: + 49 6151 16 6347

Fax: + 49 6151 16 6346

Email: riedel@materials.tu-darmstadt.de

Dr. rer. nat Emanuel Ionescu (Master advisor)

Fachbereich Material- und Geowissenschaften, Technische Universität Darmstadt

Jovanka-Bontschits-Strasse 2, 64287 Darmstadt, Germany

Tel: + 49 6151 16 6344

Fax: + 49 6151 16 6346

Email: ionescu@materials.tu-darmstadt.de